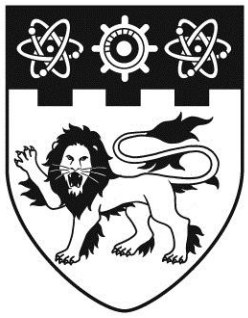

NANYANG TECHNOLOGICAL UNIVERSITY

ATTRITION OF MATERIALS IN FLUIDIZED BED

ATTRITION OF MATERIALS IN FLUIDIZED BED

ZHAO HAN

ZHAO HAN

SCHOOL OF CHEMICAL AND BIOMEDICAL ENGINEERING

2016

2016

ATTRITION OF MATERIALS IN FLUIDIZED BED

ZHAO HAN

School of Chemical and Biomedical Engineering

A thesis submitted to the Nanyang Technological University
in partial fulfillment of the requirement for the degree of
Master of Engineering

2016

Acknowledgment

Two years of my master program nearly comes to an end. It is a fruitful and thrilling adventure which full of challenges and rewards. Hence I would like to take the chance to thank those people who ever help me in all ways. If it is not for their kind help or support, I would have not reached where I am today. The fruitful results are not only for me but also for them.

First of all, I would like to extend my gratitude to my supervisor, Assoc. Prof. Raymond Lau Wai Man. I want to thank for his support, encouragement, as well as great patience. He is an approachable, humble person and always willing to spend some time discussing with me about my project. I want to thank him for his kind and easy-going gesture. If it is not for his valuable suggestion and guidance, I would not have achieved what I have achieved today.

Secondly, I want to thank all my group members who ever help or teach me in their own ways. They are Dr Wang Yabo, Dr Pei Wenbo, Dr Chen Xue, as well as Phd students AMIR FARIZHANDI. I also want to express my gratitude to my friends Andy Cahyadi, Chen Xiaoping, Huang Tan as well as Liu Ye. They either give me good advice in research or help with some tests.

Next, I want to thank my family for their moral support, encouragement as well financial support.

Last not least, I want to thank the school of Chemical and Biomedical Engineering for giving me chance to pursue my degree in NTU.

Table of Contents

Contents

List of Figures5

List of Tables 6

Abstract ……7

1. Introduction 8

2. Literature Review 9

2.1. What is attrition? 9

2.2. Sources of particle attrition 10

2.2.1.Particle attrition in the area near gas distributor. 11

2.2.2.Particle attrition in the bed of bubbling fluidized bed. 12

2.2.3.Particle attrition inside cyclone. 12

2.3. Various factors affecting particle attrition. 13

2.3.1.Particle Properties. 13

2.3.2.Design and operating conditions of fluidized bed system. 15

2.4. Hardness 18

2.4.1.Scratch hardness 18

2.4.2.Indentation hardness 18

2.4.3.Rebound hardness 19

2.5. Incinerator Bottom Ash (IBA) 20

2.6. Granular Activated Carbon (GAC) 21

2.7. Silicon Dioxide (SiO_2) 22

2.8. Calcium Sulfate 22

3. Objectives 24

3.1. Study of the effect of glass beads on attrition of IBA 24

3.2. Study of the effect of gas velocity and hardness on attrition of three materials (activated charcoal, gypsum and silicon dioxide) 24

4. Methodology 25

4.1. Study of effect of glass beads on attrition of IBA 25

4.2. Study of the effect of gas velocity and hardness on attrition 28

5. Results and Discussion 30

5.1. Result and discussion of IBA 30

5.1.1.The change of mass with time and its relation to IBA structure. 30

5.1.2.Attrition of IBA on each size range 31

5.1.3.The effect of glass beads on attrition of 1.4-1.7 mm IBA 32
5.1.4.The effect of glass beads on generation rate of fine IBA 35
5.1.5.The effect of glass beads on mass fraction of IBA 36
5.2. Result and discussion of three materials ($CaSO_4$, SiO_2, GAC) 39
5.2.1.The effect of gas velocity on attrition of materials ($CaSO_4$, SiO_2, GAC) 39
5.2.1.1.Remaining mass of $CaSO_4$ at three different velocities after 20 hours 39
5.2.1.2.Attrition of 1.4-1.7 mm of $CaSO_4$ particles with time at three different velocities 40
5.2.1.3.Generation of fines of $CaSO_4$ at three different velocities 41
5.2.2. The effect of hardness of attrition of material 42
5.2.2.1.Remaining mass of $CaSO_4$ at three different velocities after 20 hours 42
5.2.2.2.Attrition of 1.4-1.7 mm particle of three materials with time 44
5.2.2.3.Percentage of change of 1.4-1.7 mm of three materials 47
5.2.2.4.Generation of fines of three materials with time (20 h) 48
6. Conclusions 50
7. Reference 52

List of Figures

Fig. 1. Different mechanism of particle attrition [12]. 10
Fig. 2. Schematic diagram for experimental setup. 26
Fig. 3. IBA mass change of each particle size range with time (25 % small glass beads). 30
Fig. 4. The ratio of remaining mass to initial mass (W_{min}/W_0) of all size ranges (pure IBA) at U_g=1.3 m/s. 31
Fig. 5. The percentage of remaining mass over initial mass (W_{min}/W_0) of 1.4-1.7 mm IBA particles at end of 20 hours. 33
Fig. 6. The percentage of total mass change of 1.4-1.7 mm IBA across four different operating conditions at different times. 33
Fig. 7. The percentage of total mass change of fine IBA across four different operating conditions at different time. 35
Fig. 8. Mass fraction of five particle size ranges at end of 20 h for three operating conditions (pure, 25% small, 25% medium). 36
Fig. 9. Mass fraction of fine IBA across three operating conditions with time. 38
Fig. 10. Remaining mass of $CaSO_4$ at three different velocities (0.84 m/s, 1.04 m/s, 1.34 m/s) after 20 hours. 39
Fig. 11. Remaining mass of charcoal after 20 hours. 40
Fig. 12. Attrition of 1.4-1.7 mm of $CaSO_4$ particles with time at three different velocities. 41
Fig. 13. Generation of fines of $CaSO_4$ under three different velocities. 42
Fig. 14. Remaining mass of three materials (activated charcoal, gypsum and silicon dioxide) after 20 hours. 43
Fig. 15. Attrition of 1.4-1.7 mm particle size of three materials with time (20 h). 44
Fig. 16. Attrition of 1.4-1.7 mm particle size of three materials with time (5 h). 45
Fig. 17. The percentage of total change of 1.4-1.7 mm of three materials with time (5h). 47
Fig. 18. Generation of fines of three materials with time (20 h). 48

List of Tables

Table 1. Physical properties of common activated carbon used in gas-phase processes [52]. 21
Table 2. Mechanical properties of silicon dioxide [58]. 22
Table 3. Properties of calcium sulfate [60]. 23
Table 4. Compositions used for solid phase in experiments. 26
Table 5. Standardized starting particle size composition. 28
Table 6. Different gas velocities and corresponding volumetric gas flow rate for each material. 29
Table 7. Mass change of CaSO4 with time (20 h) in the air. 45

Abstract

In order to resemble ball milling process which shows better performance in moving heavy metal in incinerator bottom ash (IBA), two sizes of glass beads (0.212-0.6 mm and 0.6-1.0 mm) are utilized to co-fluidize with incinerator bottom ash (IBA) in lab scale fluidized bed at constant gas velocity (1.3 m/s). Current study focuses on the effect of different sizes of glass beads on attrition of IBA, as well as the effect of different compositions of glass beads. The results reveal that both sizes of glass beads enhance the overall attrition rate of IBA, and improve breakage of the largest sized particle. In term of fines, small glass beads will play marginally higher effect on attrition at an initial stage than medium glass beads due to larger contact surface area; however, big glass beads show more attrition at the end of the run possibly due to higher energy per unit area. Additionally, the effects of three gas velocities and hardness on attrition of three materials (activated charcoal, anhydrous gypsum, silicon dioxide) are also investigated. Results show gas velocity has effect on attrition of biggest size range of materials, despite no noticeable effect on attrition of other size ranges has been found. Furthermore, attrition will decrease with increasing the material hardness. In the size of 1.4-1.7mm, attrition of charcoal is vigorous and smooth while the attrition of silicon dioxide and anhydrous gypsum are similar in the beginning and different at later stage. It is due to large formation of subsurface crack in gypsum and little formation in silicon dioxide. Generation of fines will increase with decreasing material hardness. Mechanisms concerning different behaviors are revealed.

1. Introduction

Singapore has undergone a rapid economic development and population growth in the past 40 years. The amount of solid waste has increased rapidly and it reaches ± 7 million tons per year, which is almost 7 folds larger than that of 70s [1]. Incineration is an efficient way to reduce solid waste problem, because it may reduce the volume and mass of waste up to 90% and 70%, respectively [2-4]. Incineration bottom ash (IBA), which accounts for 80% of the incinerator residues is commonly recycled and used in landfill, cement production, and road construction [3]. It should be noted, more than 80% of the heavy metals (HMs), such as Fe, Cu, Cr, Pb, Zn, As, Ni, and Ti in municipal solid waste (MSW) were found to remain in incinerator bottom ash (IBA) after incineration [5-8]. The presence of high content of heavy metal possesses an environmental hazard. In addition, IBA consists of 15% non-combustible materials, while the remaining 85% contains 25% opaque glass and 20% isotropic glass [9].

There are some research about the physical and chemical properties of IBA in other countries [10]. The results revealed that IBA particles have average density of 2847 kg/m^3 and average circularity of 0.67 [11]. Si, Ca, Fe, Al, Zn, Cu and Ti are found to be major heavy metal components inside IBA mixture [11]. Interestingly, only few studies were found on the mobility of heavy metal during particle size reduction process. Size reduction of IBA particles can happen throughout the transportation, compaction, and blending in re-utilization process. There is a recent research dedicated to study the mobility of heavy metal during particle size reduction by ball milling and fluidization [11]. Specifically, particle size distribution, particle density, particle circularity, as well as the content of heavy metal inside bulk IBA were investigated at different stages of particle size reduction process. The mobility of heavy metal among certain particle size ranges were compared using two particle size reduction equipment, namely, ball mill and fluidized bed. In term of the mobility of heavy metal, Cu and Zn were concentrated in the IBA size of 1.0-1.4 mm, while Ti was concentrated in particle size smaller than 1.0 mm. Generally speaking, ball mill demonstrates higher efficiency in moving heavy metal than fluidized bed [11].

2. Literature Review

2.1. What is attrition?

Attrition of particle is disintegration and shrinkage processes of particle due to relative moment among particles. This phenomenon can found in various places in industry, such as inside chemical reactor or phenomenon of dust generation during particle reduction and transportation processes. Attrition of particles inside fluidized bed is mainly due to two sources, i.e., particle-particle collisions and particle-wall collisions. The straightforward consequence of particle attrition is the generation of fines which lead to mass loss [12]. This undesirable phenomenon affect the overall performance of fluidized bed (e.g., elutriation rate, bed heat transfer, reaction's selectivity and conversion) [12] due to its adverse effects, i.e., scraping inner side of wall column, reducing mean particle size [13, 14], destroying valuable particles (catalyst in fluidized bed reactor) [15], changing particle size distribution and system's hydrodynamic, and increasing the amount of fine particles and cyclone loading [16].

The complexity of particle attrition phenomenon is mainly owing to two reasons. Firstly, attrition happens on three geometry and time levels, i.e., sub-particle (e.g., particle fracturing, etc), particle, and system levels [17]. In other word, particle attrition is a function of particle type, spatial position inside fluidized bed column, column set up, as well as operating conditions (i.e., fluidization regime, superficial gas velocity, etc).

Secondly, particle attrition usually comprises of two simultaneous mechanisms, namely, particle fragmentation and particle abrasion [18-20]. Collisions may result into particle friction which gives rise to particle abrasion or particle breakage, and favors particle fragmentation. Particle fragmentation mechanism means mother particles disintegrate into identically smaller son particles, which reduces particle mean diameter, and broadens particle size distribution (PSD) width. In contrast, particle abrasion mechanism, which denotes the scraping process of irregular particle's surface into rounder particle and a lot of elutriable fine powders, produces bimodal PSD with slightly-shift PSD towards smaller mean diameter and accumulation of fine PSD. Although both of these mechanisms and the extent of attrition are function of material properties, process design, and process conditions, previous studies also found complete particle abrasion or fragmentation during fluidization [18, 19]. The lower

energy threshold of particle abrasion can explain the existence of purely abrasion-based attrition process [12]. It is necessary to evaluate particle fragmentation or abrasion process separately [13]. The evaluation of particle attrition mechanism under various circumstances is usually determined from the change of bed PSD.

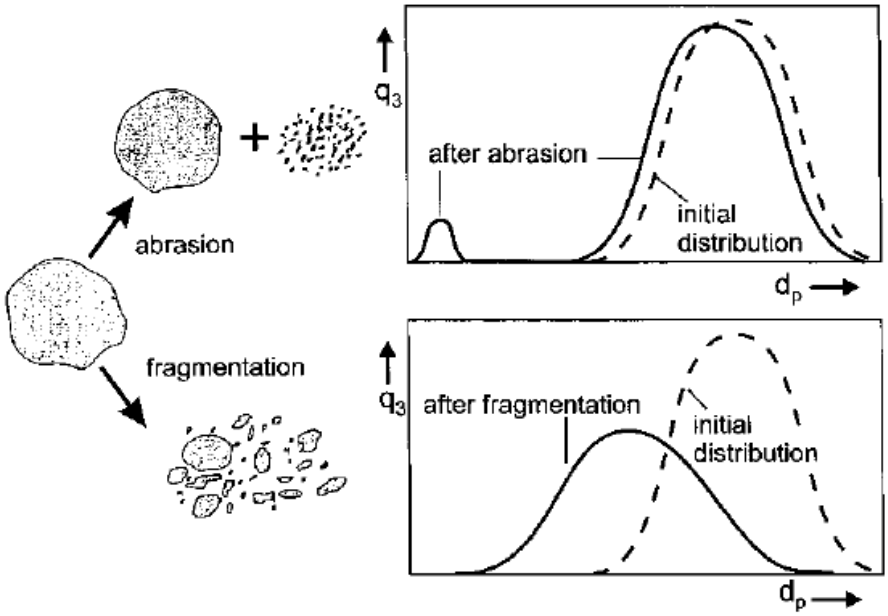

Fig. 1. Different mechanism of particle attrition [12].

2.2. Sources of particle attrition

Various locations inside fluidized bed column have been found to give different stress magnitude on particles and produce different attrition mechanism [21]. Interestingly, almost all of the attrition rate correlations for different fluidized bed locations are developed from the assumption that only abrasion process contributes to the overall particle attrition. Previous study accentuated that area near distributor, particle bed under bubbling fluidization, and cyclone are the most prominent locations for particle attrition [19]. The contribution of these locations towards total particle attrition is dependent on the operating condition. It has been found that jet-induced attrition is the most dominant factor at lower superficial gas velocity (< 0.55 m/s), while at higher superficial gas velocity, attrition in cyclone determines overall attrition in the system [12]. Although total attrition increases with superficial gas velocity, the degree of change of cyclone-induced attrition toward superficial gas velocity is bigger than jet or bubble-induced attrition [22]. Accordingly, among various attrition sources, bubble-induced attrition is the least sensitive with change of superficial gas velocity [22].

In order to study attrition process in fluidized bed system, two important factors worth to be mentioned here. First, calculation for the total attrition phenomenon inside fluidized bed column should be done separately by evaluating different attrition models at different locations of the system. Second, dominant attrition mechanism (either particle abrasion, surface cracking, or fragmentation) will be different for different operating condition, even for the same system set up and fluidized bed location. Nevertheless, these two reasons also have been pointed out as the main sources of discrepancy between empirical results of previous experimental studies [12].

2.2.1. Particle attrition in the area near gas distributor.

Perforated or nozzle plate is often made into gas distributor of fluidized bed. Smaller opening gas distributor gives higher pressure drop and uniform cross sectional gas distribution, which increase fluidization quality. On the other hand, such design will lead to formation of gas jet at high velocity, which will carry over some particles, increases particle acceleration, and overall hydrodynamics of fluidized bed suspension. Impact stress from jet towards particle bed is similar to jet grinding process [23]. This attrition mechanism is enclosed in certain area, i.e., only particle bed located below and around jet length will be affected. In most cases, bed height is usually higher than jet length. Particle attrition is constant for area above jet length. In reality, bubbles always present with jets inside fluidized bed, hence previous investigation on the jet-induced attrition also included the contribution of bubbles on particle attrition [18, 23-25].

In order to study the mechanism of jet-induced attrition separated from overall attrition phenomenon, two different methods were adopted in previous studies. The first method used extrapolation of attrition data in the surface of bed particles into bed depth where jet can be found [26, 27]. This method assumes linear relationship between attrition in the bed surface and that inside bed particle, where jet attrition induces particle deformation. However, this method is lack of comprehensive study of attrition mechanism. Second method used of modified distributors (porous plate and porous plate with nozzle) [28]. The result of particle attrition from the use of porous plate (bubble-induced-attrition) will be compared with the result from porous plate with nozzle in which jet velocity can be controlled. This method allows investigation

on the effect of purely jet-induced attrition due to over simplification that bubble velocity is constant regardless of the magnitude of jet velocity. Particularly, this method only applies to the investigation of jet attrition at low jet velocity condition. Furthermore, it has been found that horizontal and vertical jets induced the same attrition effect [28].

2.2.2. Particle attrition in the bed of bubbling fluidized bed.

Bubbles cause particle attrition by generating low-velocity inter-particle collisions. Average bubble moves with low velocity (in the order of 1 m/s) hence it is unlikely that bubble will disintegrate particles into smaller pieces [12]. As in the case of jet attrition, two different methods were also used to separately investigate the extent of bubble-induced attrition: (i) use of porous distributor to avoid jet formation [12], and (ii) measurement of fine production rate by changing static bed height to eliminate the effect of jet formation [26, 27]. Despite the abundant amount of research related to bubble-induced attrition phenomenon, no common agreement can be found for the mechanism of bubble-induced attrition inside fluidized bed.

Particle abrasion during bubble-induced attrition is affected by particle properties, i.e., particle shape, surface roughness, etc. Bubble-induced attrition rate is also affected by operating condition, i.e., excess gas velocity or the differences between superficial gas velocity and minimum fluidization velocity [16, 22, 29]. Furthermore, minimum superficial gas velocity needed to induce particle attrition is assumed to be equal to minimum fluidization velocity.

The significant effect of bed height on bubble-induced attrition is not fully understood yet. Previous experimental work showed the increase of attrition rate with bed height is due to the increase of bubble size at higher axial position [30], while the other researchers [13, 16] found the opposite result. Ray et al. [14] explained such conflicting results due to the differences in fluidization regime, i.e., bubble (slug) size is constant at any axial position for slugging regime thus it appears as bed height has no effect on particle attrition.

2.2.3. Particle attrition inside cyclone.

Another possible source of particle attrition in current study is particle attrition in cyclone. Cyclone has been found to greatly affect particle size distribution [19, 31,

32]. Particle attrition in cyclone happens due to the addition of kinetic energy which overcomes particle surface energy [20]. Cyclone attrition rate is related to particle properties and gas velocity at the entrance of cyclone [20].

It is worth to be noted that particle attrition in cyclone mostly comes from particle abrasion mechanism. Fragmentation-based attrition inside cyclone is minimum because high inlet velocity is avoided in the operation of industrial cyclone to minimize cyclone pressure drop [12]. Furthermore, increase of particle concentration has been found to decrease the probability of particle-wall cyclone collisions.

2.3. Various factors affecting particle attrition.

As mentioned before, particle attrition could be influenced by material intrinsic properties (particle shape, particle size distribution, hardness), equipment set up, and operating conditions (gas velocity). Particle attrition rate changes spatially and temporally due to chemical and/or physical interactions between particles and their surrounding [20, 33].

2.3.1. Particle Properties.

a. Particle structure.

Particle structure is considered to be most fundamental particle properties with regard to particle attrition phenomenon. Particle structure (i.e., crystal, amorphous, or agglomerate) will greatly affect both attrition degree and attrition mechanism. [12]. Various types of material will have different degree of imperfection, cracks, or dislocations, which will result in the breakage of material from a material science point of view. Crystalline material breaks more uniformly because the stress on particle is distributed evenly [14]. Amorphous particles (e.g., coal, limestone) were also studied and attrition of such materials have been found to be independent of initial bed particle size distribution and operating conditions [13, 29], presumably due to internal fractures inside their structure which dictates the final bed PSD for the-more-dominant particle fragmentation mechanism [14]. Smaller particle has less internal fractures [12]. Abrasion dominance mechanism is more common for fluidized bed reactors which utilize catalysts made from spray drying process [28].

b. Particle size and particle size distribution.

In a more dominant particle abrasion process, previous studies indicated that particle attrition increases with increase of particle size [29]. Small particle is less likely to have imperfection like micro-cracks or flaws. It is well studied that it will take a remarkably higher stress to break a small particle. The flaws or micro-cracks in small particles will also be in small size which will give rise to brittle to plastic transition and hence the small particle will become tough [34]. Another parameter that will affect the attrition is particle size distribution. Particle size distribution is closely related to volume specific surface area of the bed material. It is not only a representative of surface area that is prone to attrition but also define specific surface energy available for attrition. For instance, for a bed which consists of finer material will have much larger total surface area, however, given energy provided is constant, the energy acting on unit surface area will decrease. This theory is consistent with the result of previous researcher [29] who investigated coal attrition in mixture with unbreakable sand, it is found the attrition rate of coal increase when sand size is increased. It implies that the energy actually is shared out between material surfaces but big size will result in smaller surface area so the energy acting on unit surface area is higher [29]. In one research, in an abrasion dominating attrition experiment, the production of fines is also revealed to be in linearly relationship with particle size [20]. However, other research found out conflicting results in which increasing of attrition is found with decreasing in average particle size. Because for same weight basis, small particle which will result in large amounts of particle that will increase the chance of impacting thus enhancing attrition [35].

c. Particle shape and surface roughness.

In terms of attrition, particle surface properties can be simplified into two categories, i.e., macroscopic (particle shape) and microscopic properties (particle surface roughness). For those particles who has lower particle sphericity or higher particle surface asperities is more prone to attrition [20]. Irregular particles with multiple sharp edges or rougher particle surface are more prone to be scraped during collisions before they get rounder and smaller with time [20]. Particle surface changes gradually during abrasion process, but instantaneous change also found for fragmentation of internally-fractured particles [20].

d. Particle strength and toughness.

It is well known that it is easier to break soft material than harder material. Brittle materials can fracture or fragment easily when they are under stress, while the material with high toughness will absorb the energy before they reach the last breaking point. Strong material is not necessarily equivalent to tough material like ceramic which is strong enough but it is brittle rather than tough. Tough material does not mean they are strong enough. Instead, tough material is a trader-off between strength and ductility which can measure the material itself is ductile or brittle.

e. Fines.

In a particle abrasion dominant process, previous study shows that particle attrition will enhance with the absence of fines [36]. In other words, attrition rate will decrease with production of fines, two researchers found out this "cushioning effect" by studying the degradation of FCC catalyst. The presence of fines is thought to behave like a cushion which limit the force of collision impact and thus reduce the attrition of coarse particles. This step is also a self-controlling step which means attrition produce fines and fines inhibit the attrition in turn. However, other researches are more willing to make assumption that the fines once produced from attrition will be immediately elutriated from the system thus its effect on attrition still remains unclear [37].

f. Foreign particle.

One group who focus study on the generation of carbon fines by attrition during fluidized combustion shed light on that attrition rate will be changed by changing the size of sand [29]. The mechanism the foreign particle is affecting the attrition is still unknown.

2.3.2. Design and operating conditions of fluidized bed system.

System setups and operating conditions affect particle attrition by controlling forces imposed on individual particle. Attrition can possibly result from mechanical cause, thermal cause or chemical cause. For a laboratory scale fluidized bed alone,

particle attrition is more pronounced at higher collision frequency, longer duration time, and stronger collisions.

a. Wall surface roughness.

Similar to particle surface roughness, column surface roughness and cyclone wall roughness exacerbate particle breaking. This effect is more pronounced for bigger ratio of particle and column diameters [12].

b. Gas and solids velocity.

Mechanical stress during particle collisions is closely linked to particle properties. Particle velocity is affected by gas, bubble, or jet velocity. Higher velocity differences between two embodies which collide to each other (i.e., particle-particle or particle-wall column) will increase inter-particle momentum transfer during collisions. Some results already reveal that the attrition rate is approximately in linearly relationship with excess gas velocity above minimum fluidization velocity [29]. Particle attrition is more distinct at bottom column (area near distributor) where more bubbles and jets are present [12]. Inevitably, instantaneous hydrodynamics instability, such as jets, also aggravate particle's breaking both in short and long term due to its severe impact on particle surface morphology and surface cracking, respectively [20].

c. Particle residence time.

Higher particle residence time assures more inter-particle and particle-wall collisions. However, attrition rate showed plateaus increase with time in batch system [13, 28, 38-40]. This phenomenon related to the change of particle surface morphology along the time, whereby initial conditions with rougher surface and more irregular particle shape are less found after continuous collisions. Although collisions still happen, smaller particles with more rounded and smoother particles are less likely to particle shrinking. Above this condition, attrition rate is relative constant and only particle abrasion can be found inside fluidized bed system. This trend is hard to be found in continuous process due to the particle residence time distribution, i.e., different particle has different residence time inside fluidized bed column hence different change of attrition rate along the time. Overall attrition rate is constant but

individual particle attrition rate indicates plateaus increase over time in continuous system [12].

d. Temperature and pressure.

Temperature affects particle attrition through three mechanisms: inducing thermal stress on particles, affecting particle properties (e.g., elasticity, hardness, strength), and changing gas density [12]. Thermal stress gives rise to particle cracking due to decrease of moisture content inside particles and different thermal behavior of particle material and impurities inside it. At low temperature, particle will have plastic to brittle transition thus become brittle. On the contrary particles may soften and melt to form aggregates at higher temperature. Change of gas density due to temperature or pressure change induces different hydrodynamics condition inside fluidized bed column hence different attrition rate. Pressure instability may have more detrimental effect on particle attrition.

e. Chemical reaction.

Chemical reaction at particle surface or pores leads to surface cracking. Chemical deposition at particle surface also change particle's mechanical strength [40].

2.4. Hardness

Hardness affects attrition and particle cohesion, among other factors which affect fluidization. Hardness is intrinsic-mechanical property used to define material resistance towards plastic deformation due to compressive and/or abrasive forces [41, 42]. It is important to differentiate hardness and grindability of material. Although both material properties are important in comminution and attrition process, the latter is quantified with Hardgrove Grindability Index (HGI) using standard test ASTM B409-71 [43]. Plastics are difficult to be grinded (high HGI index), while plastics are prone to abrasive forces. Ceramics, concrete as well as some metals are commonly knowns as hard material.

2.4.1. Scratch hardness

There are three types of hardness test, i.e., scratch hardness, indentation hardness, and rebound/dynamic hardness. Scratch hardness test is commonly used in mineralogy as indentation test is preferred for metal [42]. In scratch hardness test, the surface of material is tested through friction with sharp-edge of harder material (i.e., hardness of 20 % higher or more compared to test material [42]) while changing the weighting load imposed on it [44]. Both macro- (shape or sharpness) and micro-shapes (asperities at the surface) of scratching material determine the result of the test [42]. Surface cracking after the measurement shows the hardness of test material. Scratch hardness is measured with sclerometer and the result is standardized in Mohs' scale of hardness, whereby bigger number means higher material resistance towards plastic deformation [44]. The Mohs scale hardness of minerals can be commonly found in reference sheets. Mohs' scale is ranging from 1 to 10, whereby the first and the latter show the hardness of talk and diamond, respectively. [41, 42]. Organic particles have relatively lower hardness compared to inorganic ones. Material with small Mohs scale is lower in cohesion force and higher in attrition rate [43].

2.4.2. Indentation hardness

Indentation hardness test uses fixed weighting load and specific shape of compressing material to perform indentation on the surface of test material [45]. The depth or area of indented surface directly related to tensile strength of such material

[46]. Among available indentation hardness tests, Vickers and Knoop tests are widely used in academic world while Brinell and Rockwell hardness tests (ASTM E-18) are more favorable in industry [42, 45]. Brinell test is one of the oldest hardness characterization method using 3000 kgf of spherical compressing material [42]. The shortcoming of this method is the estimation of indented diameter at test material surface (*d*) is needed to choose the appropriate diameter of compressing ball (*D*) such as their ratio (*d/D*) is between 0.3 and 0.4 [42]. Such criterion is needed to standardize the result of indentation hardness test using different weighting loads and compressing ball diameters. In order to surpass this limitation, Rockwell test uses conical compressing material, while Vickers and Knoop tests apply pyramidal compressing material. Compressing material is located at certain angle compared to test material surfaces, i.e., 120 ^{o} or 136 ^{o} for Rockwell and Vickers tests, respectively [42]. Knoop test can be used to evaluate the impact of crystal structure towards material hardness. Both indentation and scratch hardness indicate plastic, rather than elastic, properties of certain material.

2.4.3. Rebound hardness

Rebound or dynamic hardness indicates the elasticity of test material. Scleroscope converts the bouncing height of test-hammer after dropping from a known height into material's hardness [47]. There are two commercial tests can be used for such method, i.e., Leeb test and Bennet test.

2.5. Incinerator Bottom Ash (IBA)

IBA samples were collected from Tuas Incineration Plant (TIP). Screening was first conducted in order to eliminate big particles. 150 g IBA was then separated into 9 particle size ranges using sieves of mesh sizes 0.212 mm; 0.6 mm; 1.0 mm; 1.4 mm; 1.7 mm; 2.8 mm; 4.0 mm; 5.6 mm. The average circularity was found to be 0.670 derived from irregular-shaped aggregation of IBA during the incineration process. There is insignificant difference among different size ranges. The density of the pre-dried samples was also determined for different particle size ranges by a pycnometer (Quantachrome Ultra-Pycnometer 1000) in 15 runs each. The average particle density of bulk IBA was found to be 2847 ∓ 159 kg/m^3. There is not big variation across particle size ranges. Particles within size range of 1.4-1.7 mm were found to have biggest density while fines which is smaller than 0.212 mm has smallest density. Relatively high content of metal oxide possibly contributes to high particle density in size range of 1.4-1.7 mm. Considering the exceedingly high energy requirement to fluidized large IBA particles and also given that large particles do not contribute to the accumulation of heavy metal, IBA particles only less than 1.7 mm were selected to use [48].

2.6. Granular Activated Carbon (GAC)

Granular activated carbon (GAC) is highly porous mili-sized particles (i.e., > 0.18 mm according to AST D2652-74 standard, or mean particle diameter between 1 – 5 mm [49]) which mostly used in adsorption process due to its high internal surface area (i.e., > 400 m^2/g, typically 500-1500 m^2/g [50]). The high internal surface area indicates the dominant micro-pore (usually slit shape with pore size < 2 nm), while other type of internal pores such as meso-pore (2-50 nm) and macro-pore (≥ 50 nm) are also presented [51]. Activated carbon is reported to have mohs scale of hardness ranging from 1-2. The typical physical properties of activated carbon used in gas-phase processes can be found in Table 1 [52]

Table 1. Physical properties of common activated carbon used in gas-phase processes [52].

Properties, Unit	Magnitude
Bulk density, kg/m^3	600 - 800
True density, kg/m^3	2100 - 2200
Pore volume, mL/g	0.3 - 0.7 (micro-pore) 0.3 - 1.1 (meso-and macro-pores)
Specific surface area, m^2/g	1000-1500

The high carbon content inside GAC (> 90 vol/vol %) originated from the combustion of various carbonaceous feedstocks, i.e., petrochemical (coal, petroleum coke), plant (wood, bagasse), and animal-based (manure) materials, synthetic polymers, or wastewater sludge [51]. Ash content of GAC (1-12 vol/vol %) indicated the amount of inorganic materials, such as silica (S), iron (Fe), alumina (Al), carbonates, and phosphates [53]. The porosity, pore size, as well as pore size distribution of GAC are highly dependent on the raw material and manufacturing methods. Specifically, coal-based GACs have been found to have more regular macro-pore structure, higher amount of micro-pore, and lower ash content compared to wood-based GAC [54, 55], while physical/thermal activation process (i.e., using steam or other oxidizing gas such as CO_2) produces more micro-pore, wider pore size distribution, and lower mechanical strength compared to chemical activation process [52]. Pore formation during thermal activation consists of several stages: (i) formation of micro-pore at initial burn-off stage due to vaporization of volatile organic substances, followed by micro-pore

widening which results in wider pore size distribution of micro-pore; (ii) formation of meso-pore at middle and high level burn-off stage due to the disappearance of pore wall between micro-pores; (iii) the disappearance of pore wall between meso-pores and formation of macro-pore at higher burn-off stage [56]. Chemical activation prevents particle shrinkage at higher temperature by dehydration and other crosslinking process, hence it produces pore inside carbon particles [56].

2.7. Silicon Dioxide (SiO_2)

Silicon dioxide (SiO_2) or silica is a material that exists in many crystalline form as well as amorphous state. It can be found abundantly in the mixture of beach sands in the form of quartz. [57] Silicon dioxide is the main component of glass (e.g., drinking glasses, bottles, etc) and widely used in semiconductor industry due to its high dielectric strength and good thermal and mechanical stability [58]. In this experiment, silica is in the form of a-quartz. Silicon dioxide has molecular weight of 60.08 g/mol and bulk density ranged from 2180-2648 kg/m^3. Silicon in from of a-quartz has mohs scale of hardness 7 [58]. Table 2 summarizes important mechanical properties of silicone dioxide [58].

Table 2. Mechanical properties of silicon dioxide [58].

Properties, Unit	Magnitude
Compressive strength, Pa	1.1×10^6 - 1.6×10^6
Fracture toughness, $Pa.m^{0.5}$	620-670
Hardness, Pa	$4.5 \times 10^6 – 9.5 \times 10^6$
Tensile strength, Pa	4500 - 155000
Young's modulus, Pa	$6.63 \times 10^{10} – 7.48 \times 10^{10}$

2.8. Calcium Sulfate

Calcium sulfate is inorganic compound with the formula $CaSO_4$. The compound exists in mainly two forms in nature. First form is anhydrous form (anhydrite) which is widely used as desiccant. Its mohs hardness is 3.5. Second form is dehydrate form with formula $CaSO_4$ $(H_2O)_2$. It is a soft natural occurred mineral with mohs hardness 2. Anhydrous Calcium will absorb moisture slowly to form hemihydrate (CaSO4·nH2O) at ambient condition while gypsum can also convert to hemihydrate when temperature

rises above 100 °C. Calcium sulfate has bulk density between or 2320 kg/m^3 (dihydrate) to 2960 kg/m^3 (anhydrite), with molecular weight from 136.14 g/mol (anhydrite) to 172.172 g/mol (dihydrite) and orthorhombic crystal structure [59]. Gypsum is widely used as part of cement mixture. Some of the important properties of calcium sulfate can be found in Table 3 [60].

Table 3. Properties of calcium sulfate [60].

Properties, Unit	**Magnitude**
Melting point, ℃	1460 (anhydrite)
Solubility (water, 20 ℃), kg/m^3	2.1 (anhydrite)
	2.4 (dihydrite)

3. Objectives

3.1. Study of the effect of glass beads on attrition of IBA

- To study the effect of size of glass beads on attrition or particle size reduction,
- To study the effect of composition of glass beads on attrition or particle size reduction.

3.2. Study of the effect of gas velocity and hardness on attrition of three materials (activated charcoal, gypsum and silicon dioxide)

Previous section investigates the effect of foreign particles (namely, sizes and compositions of glass beads) on particle attrition (i.e., IBA). Current section aims to investigate (1) the effect of particle harness and (2) the effect superficial gas velocity on particle attrition.

4. Methodology

4.1. Study of effect of glass beads on attrition of IBA

The previous study aimed to find out the physical and chemical properties of IBA in Singapore. The average density, circularity, chemical composition was investigated as well. Additionally, Cu and Zn element were “moved” and concentrated in the 1.0-1.4 mm range while Ti was “moved” and concentrated in size range below 1.0 mm through ball milling process and fluidization. [11] Previous study reveals that heavy metal moves across different size range and concentrate at certain size range through particle size reduction process. It is reasonable to believe that particle size reduction (fluidization and ball milling) will to some extent affect the mobility of heavy metal. Compared to fluidization process, ball milling process is shown to have more control over movement of heavy mental across different size ranges. In order to resemble the process in ball milling, the following work is to study the mechanism of attrition by introduction of glass beads in fluidized bed. In order to investigate how attrition can be altered, two different sizes of glass beads and two different compositions of these glass beads will be used to co-fluidize with IBA.

The IBA samples used in this research were collected from Tuas Incineration Plant (TIP) Singapore. The IBA samples which consist primarily of ash and residue from the combustion of domestic and industrial waste incineration were undergoing incineration at around 1000 ℃ for 2 hours. Prior to experiments, The IBA samples would be dried at 90 ℃ for 24 hours in drying oven.

The experimental setup consists of a solid-gas fluidization bed with air as the gaseous phase. A schematic diagram of the setup is shown in Figure 2. The fluidization bed column was constructed with transparent acrylic, with 30 mm in diameter and 1.2 m in length. A 2-stage separation was used to remove entrained particles from the exiting gas-stream. The removed particles were collected into a fine collector underneath the cyclone.

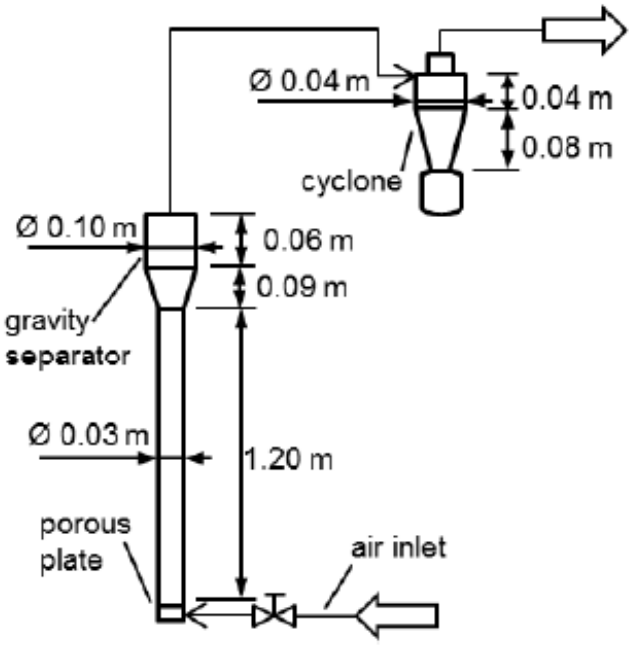

Fig. 2. Schematic diagram for experimental setup.

Subsequently, dried IBA particles larger than 1.7 mm were removed using *W.S. Tyler U.S.A. Standard Sieves* prior to all experimentation due to the unfavorable energy requirements of fluidization. Sieving also ensures minimum discrepancy in initial particle size distribution of IBA particles across all experiments. These remaining IBA particles were then weighted and gently mixed with glass beads of diameter 0.2-0.6mm (referred to as "S glass beads") and diameter 0.6-0.8 mm (referred to as "M glass beads") at predetermined mixing ratios listed in Table 4. The total mass of bed was kept at 200 g in all experiments. In this study, a total of 4 experiments were conducted with the solid phase mass compositions showed in Table 4.

Table 4. Compositions used for solid phase in experiments.

Experiment	**IBA**	**Small Glass Beads**	**Medium Glass Beads**	**Total Mass**
Pure IBA	100 %	0 %	0 %	200 g
25 % Small	75 %	25 %	0 %	200 g
50 % Small	50 %	50 %	0 %	200 g
25 % Medium	75 %	0 %	25 %	200 g

Compressed air was used as gas source. The gas was introduced into the fluidized bed with 55 L/min (1.30 m/s) measured by a *Cole & Parmer 1G08 R3 rotameter*. The flow rate was adjusted to be sufficiently higher than the minimum fluidization velocities of all 4 operating conditions. After each predefined duration (0.5 h, 1 h, 2 h, 3 h, 4 h, and 20 h), the air flow would be disconnected and samples were collected for sieving analysis from both fluidized column and fine collector. Analysis was performed by sieving the sample using mesh of 0.212 mm, 0.6 mm, 1.0 mm, 1.4 mm and 1.7 mm with amplitude of 50 µm for 15 minutes in a *Retsch AS 200 sieving machine*. Mass of particles collected on each sieve was recorded, and cumulative mass fractions were plotted against sampling time.

4.2. Study of the effect of gas velocity and hardness on attrition

Previously, IBA has a non-uniform physical properties and inhomogeneous chemical constituent. In combination with introduction of foreign particles (glass beads in this case), experiment results will be subject to big discrepancy. Hence in new study, new materials with homogeneous chemical constituent and physical properties will be used. Additionally, three physically homogenous materials but with different hardness level are chosen to be activated charcoal, anhydrous gypsum ($CaSO_4$) and silicon dioxide (SiO_2). It can be found that activated charcoal is with mohs scale of hardness 1-2, anhydrous gypsum is with mohs scale of hardness 3.5 and silicon dioxide with mohs scale of hardness 7.

Secondly, it is reported that rate of attrition is function of excess gas velocity (U_f - U_{mf}) [61]. In combination with factor of hardness, the objective of new study is to investigate the effect of gas velocity on attrition of materials with time and the effect of material property (hardness) on attrition of materials with time.

Activated charcoal, anhydrous gypsum and silicon dioxide are all procured from Sigma-Aldrich Singapore. Activated charcoal has specific density of 0.6 and initial particle size is larger than 8 mesh (2.36mm). Anhydrous gypsum has specific density of 2.9 and initial particle size is also larger than 8 mesh (2.36mm). Silicon dioxide has a specific density of 2.6 and 4-20 initial mesh size which is ranging from 4.75mm to 0.85mm. Considering unfavorable energy requirement to fluidize particles as big as 2.36mm, all three materials (activated charcoal, anhydrous gypsum and silicon dioxide) will be ground to smaller size using ball miller (Fritsch, Planetary Mill Pulverisette 5, Germany). Each grinding bowl has 80ml volume and five agate grinding balls which has 10mm diameter will be put into each bowl. In order to meet standardized initial particle size distribution shown as in table 5, three materials will be ground by different ball milling cycle time to achieve best grinding results due to different hardness but at same speed (200rpm).

Table 5. Standardized starting particle size composition.

	1.4-1.7mm	**1.0-1.4mm**	**0.6-1.0mm**	**0.212-0.6mm**	**<0.212mm**
Percentage	13.20%	19%	28%	34.60%	5.20%

Prior to any fluidization experiment, 100 gram sample of each material will be prepared according to standardized initial particle size distribution. They will be dried in oven at 90 ℃ for 24 hours to get rid of moisture.

Then it will be transferred to fluidized bed after drying. The set-up of fluidized bed is shown in figure 2. In this study, because of their different particle density, they will give rise to different minimum fluidization velocity. Hence three different gas velocities are chosen for each material respectively to make sure they are fluidized at the same excess gas velocity. The gas velocity (meter/second) chosen for each material as well as their corresponding volumetric gas flow rate (liter per minute) are shown in table 6.

Table 6. Different gas velocities and corresponding volumetric gas flow rate for each material.

	U_{mf}	U_{f1}	Q_1	U_{f2}	Q_2	U_{f3}	Q_3
Activated Charcoal	0.096m/s	N.A	N.A	0.688m/s	29 lpm	0.99m/s	42 lpm
Anhydrous Gypsum	0.44m/s	0.83m/s	35 lpm	1.03m/s	44 lpm	1.34m/s	57 lpm
Silicon Dioxide	0.41m/s	0.80m/s	34 lpm	1.00m/s	42 lpm	1.30m/s	55 lpm

In this study, compressed air was used as gas source as well. The gas was introduced into the fluidized bed with different gas flow rate shown in table 6 measured by a *Cole & Parmer 1G08 R3 rotameter*. After each predefined duration (0.5 h, 1 h, 2 h, 3 h, 4 h, 5h and 20 h), the air flow would be disconnected and samples were collected for sieving analysis from both fluidized column and fine collector. Analysis was performed by sieving the sample using mesh of 0.212 mm, 0.6 mm, 1.0 mm, 1.4 mm and 1.7 mm with amplitude of 50 μm for 15 minutes in a *Retsch AS 200 sieving machine*. Mass of particles collected on each sieve was recorded, and analyzed.

5. Results and Discussion

5.1. Result and discussion of IBA

5.1.1. The change of mass with time and its relation to IBA structure.

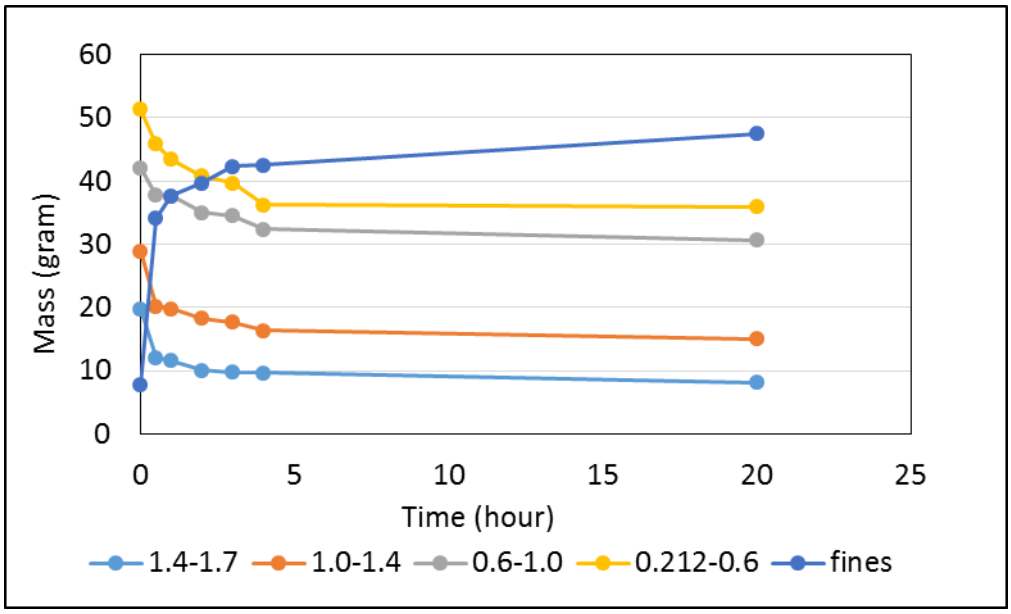

Fig. 3. IBA mass change of each particle size range with time (25 % small glass beads).

Figure 3 is a representative diagram of mass change of IBA with time at 25 % small glass beads. Each line represents the mass change of a single size range with time. It is observed that the line representing fines is constantly increasing and it increases dramatically in the first half an hour fluidization then it levels off to a plateau. The other lines representing different size ranged IBA particles decrease dramatically in the first half an hour and afterwards it decreases slowly until it reaches steady state. Under four operating conditions, the IBA mass change with time consistently shows similar plateauing manner. It should be noted that all of the experiment were run for 20 hours afterwards the attrition process is considered to be steady. The experiment was stopped and measured more frequently at initial stage. Figure 3 reveals that changes will occur rapidly during initial stage and gradually leveled off to a stable state which can be reflected by a slowly changing slope in the diagram. This result is in a good agreement with previous experimental result in the literature [61]. So it can be inferred that attrition of IBA starts with tearing off the fragile structure first by chipping away

sharp edge and corner. As reported in literature, the particles in fluidized bed will become smaller and more spherical with time, which make them less prone to attrition [37]. This explains the reason of higher attrition rate at initial stage and it decreases with time. On the other hand, cracks and dislocation inside IBA particle are more inclined to propagate at initial stage and lead to breakage of particle afterwards.

5.1.2. Attrition of IBA on each size range

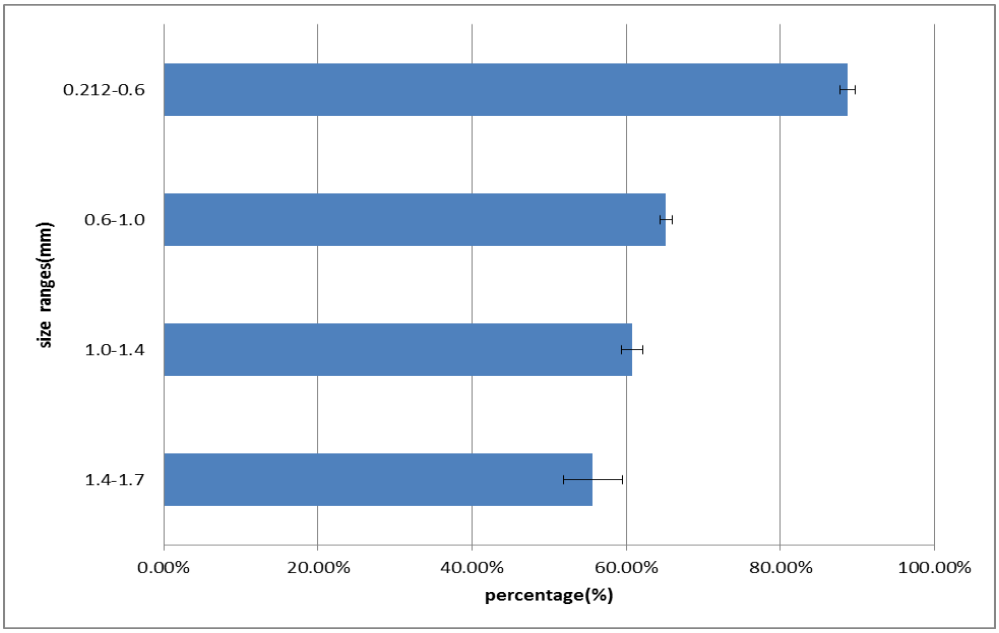

Fig. 4. The ratio of remaining mass to initial mass (W_{min}/W_0) of all size ranges (pure IBA) at U_g=1.3 m/s.

For all of the experiment, the cut-off time is set to be 20 hours as it is presumed that all experiments are approximating the steady state, i.e., attrition of particle is negligible afterwards. The remaining mass at 20 hours experiment is considered as minimum mass of each size range after particle attrition. W_{min}/W_0 is the ratio of minimum mass to initial mass of IBA. Figure 4 showcases the weight percentage of the remaining particles after 20 hours to their initial weight. It can be seen across all size ranges that bigger size range particles show higher size reduction than smaller size range particles, e.g., the weight percentage of the particles of 1.4-1.7 mm is smaller than that of 1.0-1.4 mm. Larger particles are more inclined to have micro-cracks or dislocations and thus will show higher attrition rate. Large IBA particles appear to be more asymmetric and have more surface asperity compared to small particles, hence greatly increase the chance of particle attrition. Smaller cracks will undergo brittle to

plastic transition and behave in a plastic manner hence reduce attrition [34]. On the contrary, some researchers proposed that attrition rate will decrease with particle size. Because their model suggests that attrition rate is roughly proportional to excess gas velocity exceeding minimum fluidization velocity (U_g - U_{mf}), and the particle size will only affect U_{mf} and smaller particle with lower U_{mf} will have higher attrition rate [29]. Considering such model is only dedicated for bubbling zone of fluidized bed, it overlooks the attrition in distributor area. Such model cannot be used to predict overall attrition rate under other fluidization regimes. In addition to that, the model they built is based on some assumptions which cannot represent the real situation of IBA. It is based on six assumptions while three of them are conflicting with our study. Firstly, it is assumed that every particle will have the same shape factor particle, while IBA particle naturally found in various shapes. Subsequently, previous model assumed uniform fluidization and the absence of particle segregation. However, in this study, largest particle is revealed to vibrate only at the bottom and appear segregated from other size range particles. Lastly, it is assumed particle will have steady-state attrition; however, attrition is not at steady state at first but reaches maximum at first and decreases to steady-state later. To sum up, the model they proposed is not applicable to the study of IBA.

It should also be pointed out big particles will be broken down to smaller size range. This fact will directly lead to the increasing mass of small particle. It also helps explain the reason of small change of small particle size.

5.1.3. The effect of glass beads on attrition of 1.4-1.7 mm IBA

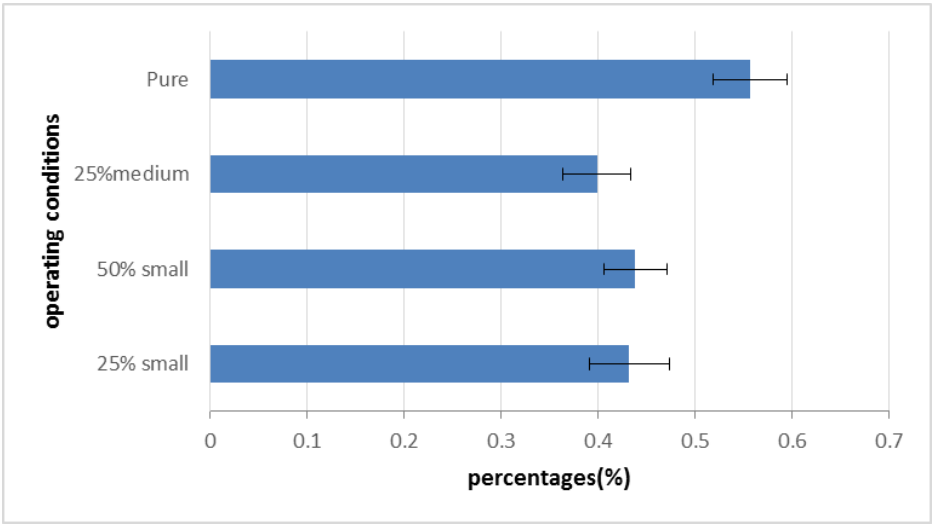

Fig. 5. The percentage of remaining mass over initial mass (W_{min}/W_0) of 1.4-1.7 mm IBA particles at end of 20 hours.

Considering mass in size range of 1.4-1.7 mm can only be destroyed but mass in other size range can be generated as well as destroyed, it is difficult to derive a theory from investigating the other size ranges. Study will be focused on size range of 1.4-1.7 mm. Additionally, after comparing each size ranges across all four operating conditions, it shows more significant reduction in the size range of 1.4-1.7 mm with glass beads than other operating conditions without glass beads. In other words, in figure 5, particles in the size range of 1.4-1.7 mm are reduced more significant under the influence of glass beads (25% medium, 50% small, 25%small). Subsequently, investigation is focused to study the effect of glass beads on rate of change in attrition process in order to further understand the impact of glass beads.

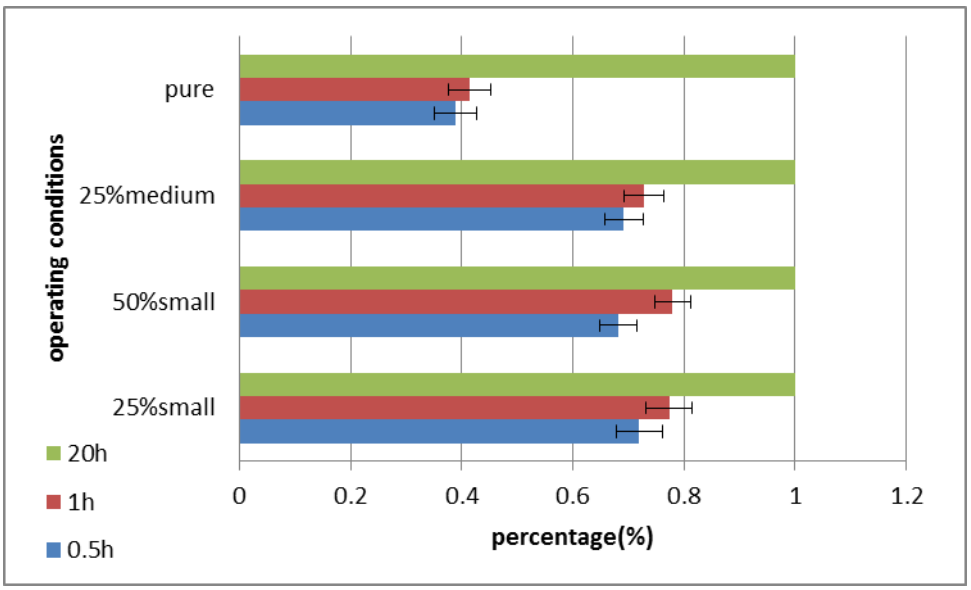

Fig. 6. The percentage of total mass change of 1.4-1.7 mm IBA across four different operating conditions at different times.

In Figure 6, the percentage of total mass change of size range 1.4-1.7 mm as x-axis is plotted across all four operating condition, i.e., 25 % small glass beads, 50 % small glass beads, 25 % medium glass beads, and pure IBA. The percentage of total mass change is defined as the ratio of mass change between beginning to preset time to total mass change across whole timescale. The length of bar represents how many percent of the change has happened until 0.5 h, 1 h, and 20 h respectively and three bars representing different time respectively are shown in groups. For instance, under 25 % small glass beads condition it will take 20 hours for total change to happen and

however, it will only take 1 hour for 80 % of the total change to happen. Most changes are found to happen at first hour. The same phenomena will be found in the case of 50 % small glass beads and 25 % medium glass beads. In contrast, for the pure IBA only around 40 % change happens at first hour. So it is reasonable to attribute glass beads to fast attrition (change) within the first hour. Given that IBA is a mixture which consists of different size range particles. The bigger particle are inclined to have more porous structure on the exterior [10]. Porous structure is amorphous and soft and easy to break. The porous structure which surrounds inner core is thus shown to be more prone to attrition by means of glass beads. Addition of glass beads is believed to introduce large impact force between IBA particle and glass beads because glass bead itself is hard and strong. Secondly it will increase the contact surface area which is exposed to attrition when small glass beads were added. Addition of small glass beads will significantly change overall particle size distribution and therefore the portion of small particles which contribute most to contact surface area per unit mass will increase greatly. Based on estimated calculation, with the same mass basis, the total contact surface area will increase by 7% when 25% small glass beads are involved in and increase by 14% when 50% small glass beads are involved in compared to pure IBA condition. In an abrasion dominant fluidized bed, attrition will start from contact surface; increased contact surface area will enhance the frequency of inter-particle collision and abrasion regardless of either IBA-IBA particle collision or IBA-glass beads collision. Additionally, compared to pure IBA condition, the presence of small glass beads will also greatly increase the chance of collision and abrasion between IBA particle and glass beads which will lead to more attrition, because glass beads are relatively hard and strong, during collision and abrasion with IBA, IBA particle is more likely to be attrited. That explains why there is more reduction in the size range of 1.4-1.7 mm with glass beads than the condition without glass beads. The effect of 25 % medium glass beads on attrition of 1.4-1.7 mm is shown to be slightly weaker than the effect of 25 % small glass beads. It is possibly due to the smaller contact surface area.

5.1.4. The effect of glass beads on generation rate of fine IBA

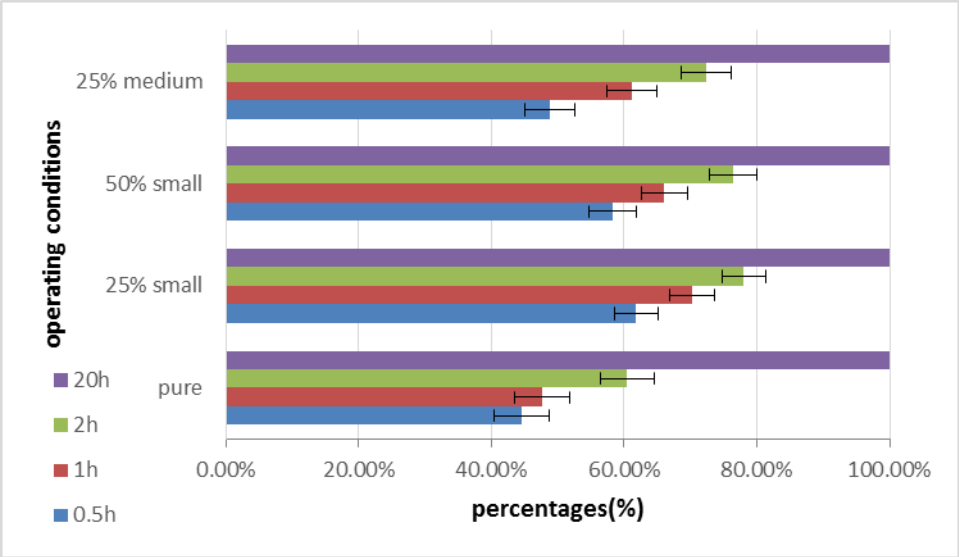

Fig. 7. The percentage of total mass change of fine IBA across four different operating conditions at different time.

In an abrasion dominant fluidized bed, fines are a direct indicator of extent of attrition. Some reports say that the elutriated particles are mostly attrited fines instead of mother particle [62]. Because of the potential fluctuation that will stem from flow pattern and compressor, it is of high feasibility to take into consideration both elutriated fines and fines captured in the collector together when considering the total fines generated. Additionally, as different operating condition starts with different IBA bed mass (the bed mass is kept the same for all experiments but IBA mass itself is not the same), it is not feasible to distinguish the extent of attrition by directly comparing the amount of fines as it is obvious that different bed mass will generate different amount of mass, it is impossible to separate the contribution the glass beads make to the fines from the contribution that different mass make. Instead of looking at how much the fine is produced, attention could be focused on seeing how fast fine is generated and how much portion of fine accounts for. The term "percentage of total change" is introduced here again. The percentage of total mass change is the amount of change between 0h to preset time over total change across the whole timescale. According to Figure 7, more than 60% of total fines are produced within first hour for the three operating conditions with glass beads, while only less than 50% of total fines are produced for the pure IBA at the same time. The same phenomena will be observed at second hour and half hour. This is an immediate evidence that glass beads

will help produce fine faster, in other words glass beads will increase overall attrition rate.

5.1.5. The effect of glass beads on mass fraction of IBA

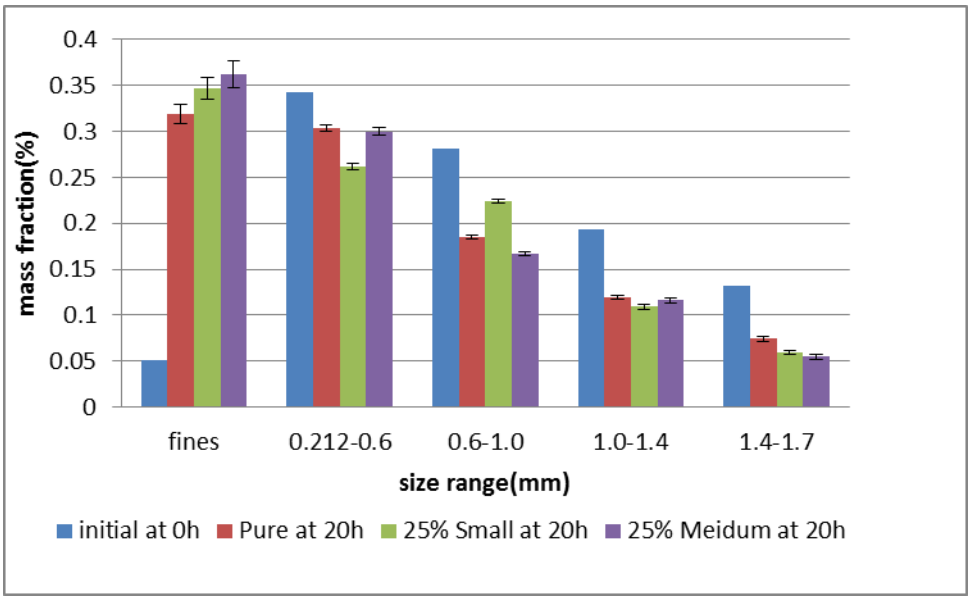

Fig. 8. Mass fraction of five particle size ranges at end of 20 h for three operating conditions (pure, 25% small, 25% medium).

Mass fraction of particle size ranges of three operating conditions at 20 h versus initial mass fraction of particle size range are shown in Figure 8 in which mass fraction is plotted against different particle size ranges. Due to inevitable experimental limitation that amount of glass beads will be stuck in one interval upper mesh, 0.212-0.6 mm sized glass beads will be stuck in one interval upper mesh of 0.6-1.0 mm likewise 0.6-1.0 mm sized glass beads will be stuck in one interval upper mesh of 1.0-1.4 mm. In view of 50 % small glass beads (0.212-0.6 mm) case, the amount of glass beads stuck in the mesh of 0.6-1.0 mm is significant and not practically separable from IBA particles. The particle size distribution will deviate from real situation due to large presence of the glass beads. Therefore particle size distribution of 50% small glass beads will not be discussed here. Even if there are still some glass beads inevitably stuck in larger mesh in the case of 25 % small glass beads (0.212-0.6 mm) and 25 % medium glass beads (0.6-1.0 mm), however, considering the mass of glass beads stuck in one interval upper mesh are insignificant to mass of IBA particle in the same mesh. For all three conditions, the mass fraction of particle sizes ranges of 1.4-1.7 mm, 1.0-

1.4 mm, and 0.6-1.0 mm were reduced to different extent with only mass fraction of fines increasing. For the size range of 1.4-1.7 mm, the condition of pure IBA shows highest mass fraction at 20 h which indicates lowest attrition rate and the other two conditions shows roughly the same percentage while for the size range of 1.0-1.4 mm, three conditions show approximately the same percentage. The first three size ranges were worth further interpretation. Since all three conditions will have exactly the same initial mass fraction in the beginning, but at end of each running 25 % small condition and 25 % medium condition still shows slightly higher mass fraction of fines. Hence glass beads are believed to increase attrition rate. Interestingly, 25 % medium glass beads will produce larger portion of fines than 25 % small glass beads. The results seem to contradict with observation before that more contact area will increase attrition rate and therefore produce more portion of fines, however, it can be interpreted from energy density (energy acting on unit area) point of view. It should be pointed out that all experiments have exactly the same operating conditions. Gas velocity and experiment running time can be regarded as two main indictors of energy supplied to the system, so it could be assumed that energy supplied externally is the same for each operating condition. Impacting energy is shared out between all material surfaces but large size particle will result in smaller contact surface area so the energy acting on unit surface area is higher therefore higher energy acting on unit area is believed to produce more fines. This finding that attrition slightly increase with particle size of foreign particle are in good accordance with what is reported in work done by Arena [29]. In Figure 9, it can be seen that 25 % small glass beads condition will produce more portion of fine at 0.5 h and 1h but 25 % medium glass beads condition gradually caught up from 3 h onwards and eventually surpass 25 % small glass beads conditions. It seems like the factor of contact surface area will become dominant at initial stage then factor of surface energy density gradually catch up and become dominant at later stage. 25 % small glass beads show more attrition at initial stage than 25 % medium glass beads. Given that attrition will always start from particle's exterior surface, it is possibly because it requires less energy to break fragile structure outside, more contact surface area will therefore give rise to more attrition and become dominant at initial stage. After fragile structure is gradually abraded off, it comes to a point where it will take more energy to break off IBA particles. It is when factor of energy density begins to dominate. Energy acting on unit area under 25 %

medium glass beads will produce more energy every collision and therefore will produce more attrition at later stage.

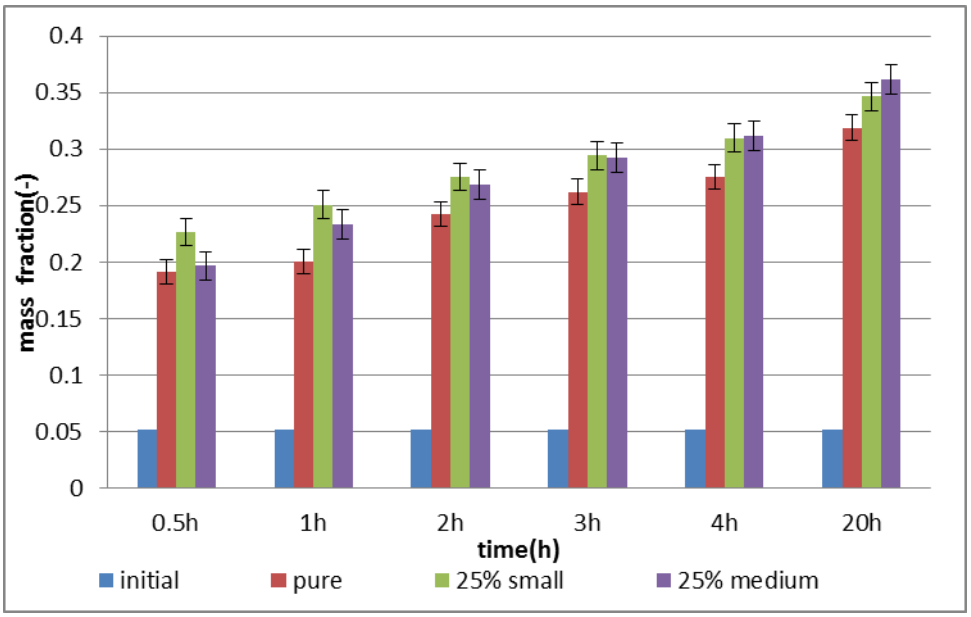

Fig. 9. Mass fraction of fine IBA across three operating conditions with time.

It is also worth noting that 25 % small glass condition will end up with lower composition of size range 0.212-0.6 mm than the other two conditions and likewise 25 % medium glass will also end up with lower composition of size range 0.6-1.0 mm. Glass beads have similar density with IBA particles and the size of glass beads is comparable with corresponding size range of 0.212-0.6 mm or 0.6-1.0 mm. It is possible that these glass beads will be fluidized in a similar manner with corresponding size ranges of IBA particles. In the course of fluidization, apart from colliding with other size ranges IBA particle, glass beads are expected to have higher chance to collide with corresponding size ranged IBA particle since they are believed to have similar manner during fluidization. Therefore it will show more attrition in corresponding size range. Likewise the other sized-particles that do not have similar behavior with glass beads will have less chance to collide with glass beads. Glass beads are relatively hard and strong compared to all IBA particles, so corresponding size ranged IBA particles will be attrited by them.

5.2. Result and discussion of three materials ($CaSO_4$, SiO_2, GAC)

5.2.1. The effect of gas velocity on attrition of materials ($CaSO_4$, SiO_2, GAC)

5.2.1.1. Remaining mass of $CaSO_4$ at three different velocities after 20 hours

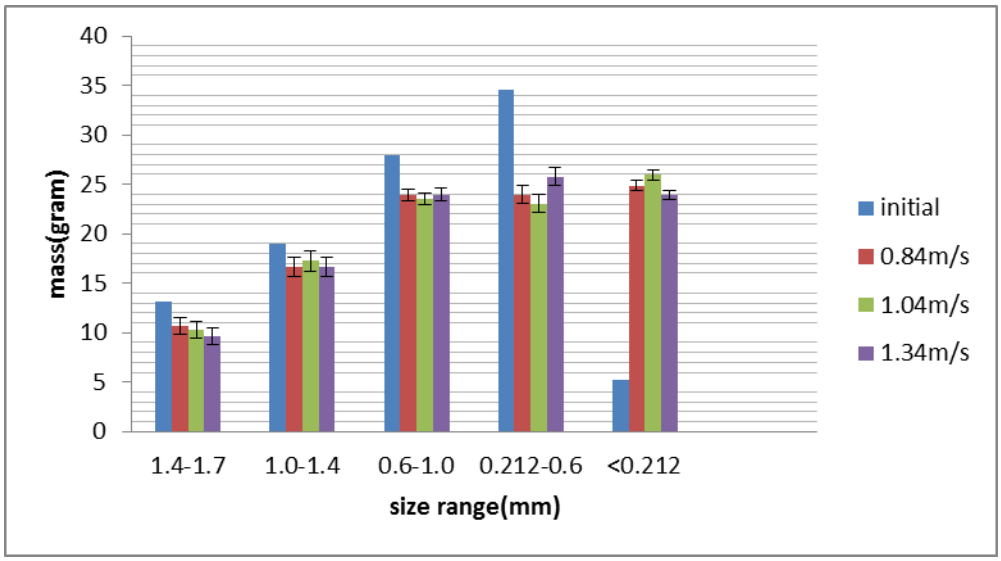

Fig. 10. Remaining mass of $CaSO_4$ at three different velocities (0.84 m/s, 1.04 m/s, 1.34 m/s) after 20 hours.

Three experiments of $CaSO_4$ are run to 20 hours at 0.84m/s, 1.04m/s and 1.34m/s respectively with exactly the same starting particle size distribution. $CaSO_4$ are deemed to approximate the steady state after 20 hours. In Figure 10, remaining mass of $CaSO_4$ in fluidized bed under three gas velocity as well as initial condition are plotted across all size ranges. It is worth noting in the size range of 1.4-1.7mm, the mass of particles appears to decrease with gas velocity. It reveals that the particles of 1.4-1.7 will be attrited more with high speed (It will be discussed in details below). While the other two size ranges (1.0-1.4mm and 0.6-1.0mm) does not show noticeable trend even if there is some difference in values. Additionally, attrition of charcoal at 0.73m/s is run two times. The remaining mass of particle size 0.212-1.7 mm is plotted against particle size range in Figure 11. It can be seen that with the exactly same operating condition it can still result in difference in values due to experiment error. It should be noted that the remaining mass of 1.0-1.4 mm particle size are 3.4 and 5.78

respectively. In the light of the fact that experimental error can result in value discrepancy as much as 1 gram when running at exactly the same operating condition, so the difference shown in the 1.4-1.0 and 0.6-1.0 as well as 0.212-0.6mm size ranges can be regarded as insignificant. It seems that that gas velocity has minor effect on attrition of these two size ranges.

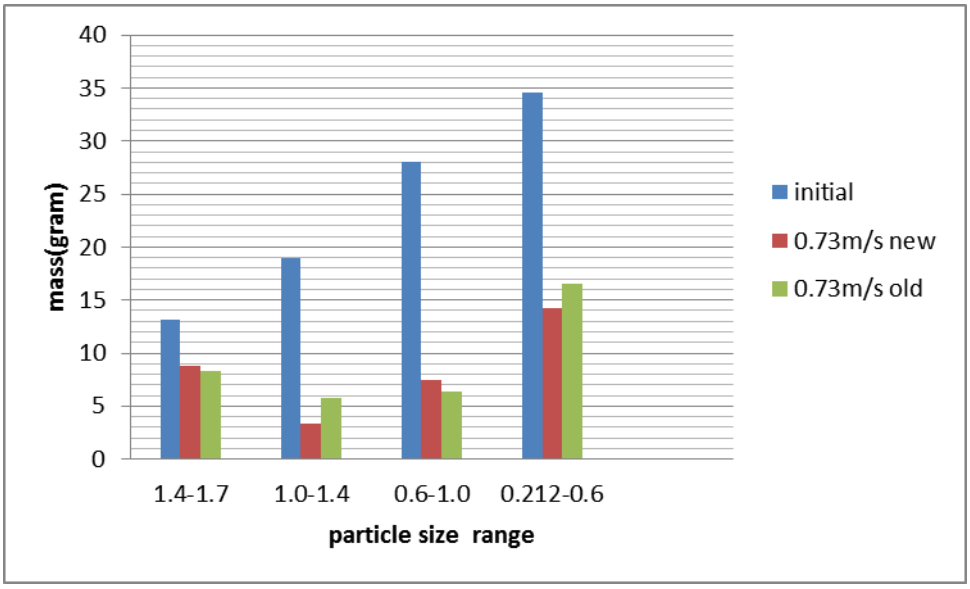

Fig. 11. Remaining mass of charcoal after 20 hours.

5.2.1.2. Attrition of 1.4-1.7 mm of $CaSO_4$ particles with time at three different velocities

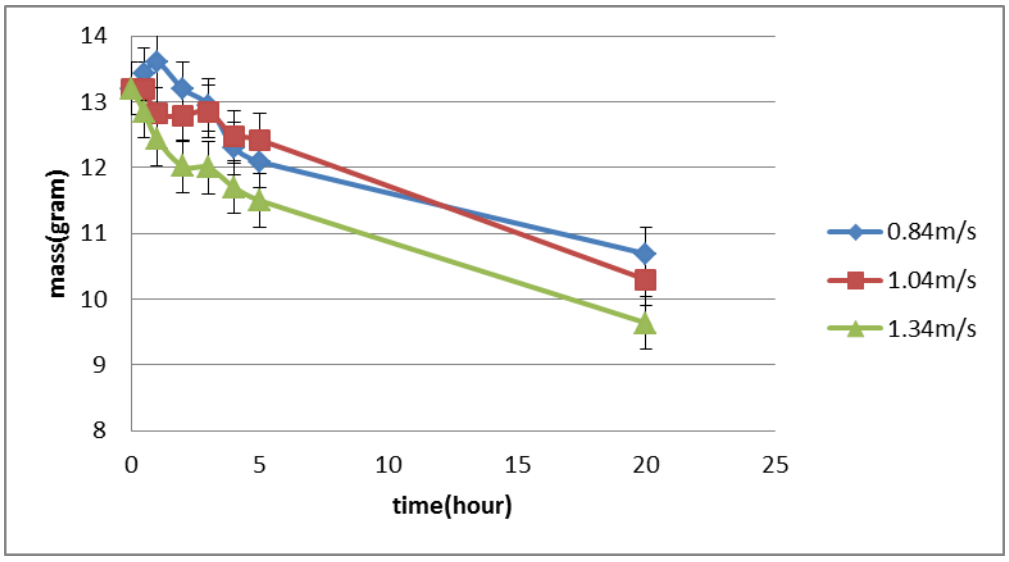

Fig. 12. Attrition of 1.4-1.7 mm of $CaSO_4$ particles with time at three different velocities.

Figure 12 shows the attrition of biggest particle size range across the whole timescale. It is more practical to study attrition of 1.4-1.7 mm particle size as it can only be attrited rather than generated. In Figure 12, it shows the attrition of 1.4-1.7 mm at 1.34 m/s is more remarkable than other two conditions in the short run. Attrition starts to decrease after the beginning. The attrition of particle at 1.04 m/s is higher than that of 0.84 m/s in the beginning and gradually level off and finally catch up with that 0.84 m/s and surpass 0.84 m/s by a small margin in the end. For 0.84 m/s condition, since anhydrous gypsum is widely used as desiccant, it will absorb moisture at ambient condition. So mass of gypsum increases at first due to absorption of moisture and starts to decrease after that before finally leveling off in a similar manner with 1.04 m/s. In comparison with mass change at 0.84 m/s, mass change at 1.34 m/s reveals higher gas velocity will increase attrition rate. It is consistent with finding in the literature [63]. There are different trends between them in the first two hours; however, mass change with time of 0.84 m/s condition is not clearly distinct from mass change of 1.04 m/s at end of run. The experimental error and moisture adsorption will affect the actual results thus reducing the effect of gas velocity. The comparison between 0.84 m/s and 1.04 m/s cannot showcase the distinct difference in attrition.

5.2.1.3. Generation of fines of $CaSO_4$ at three different velocities

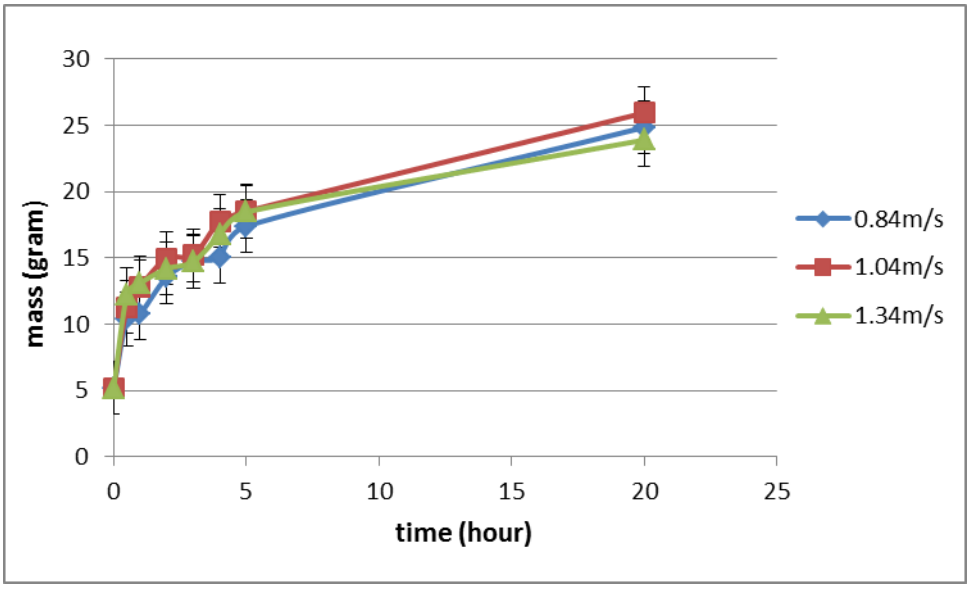

Fig. 13. Generation of fines of $CaSO_4$ under three different velocities.

The generation of fines of CaSO4 with time is shown in figure 13. It can be found the generations of fines at three different gas velocities increase in a similar manner and they all increase rapidly in the beginning and speed of increment gradually slows down. In consistent with previous IBA results and other literature [61], it indicates attrition increases rapidly in the beginning and gradually levels off to a stable state. Because attrition itself is surface smoothening process which will chip away sharp edge and corner first. Crack will also propagate at the first stage. Particles will become smoother and smaller with time which will make them less prone to attrition [37]. 1.04m/s and 1.34m/s condition shows higher generation rate of fines than 0.84 m/s condition most of time, and the two lines representing them are overlapped at some point which shows no obvious distinction, however, the fine of 0.84m/s surpass 1.34m/s at last. But all three conditions differ from each other by a small margin at end of run. Based on the results, it is safe to infer gas velocity will have effect on attrition of material to small extent. In my study, the intervals between three chosen gas velocities are not large enough so that the difference resulting from gas velocity in attrition among three different operating conditions may be not distinguishable owing to experimental errors. Experimental errors like fluctuation in flow pattern, unsteady flow rate, inhomogeneous particle shape will give rise to variations in results. Therefore, it is difficult to tell the effect of gas velocities on attrition from variations caused by experimental errors.

5.2.2. The effect of hardness of attrition of material

Attrition process itself is a complex process as discussed in literature review. Various factors will have effect of attrition of material. It was revealed that both excess gas velocity and material hardness can have major effect on it [34, 62]. In order to study the effect of hardness on attrition alone, experiments of three materials are run at the same excess gas velocity.

5.2.2.1. Remaining mass of $CaSO_4$ at three different velocities after 20 hours

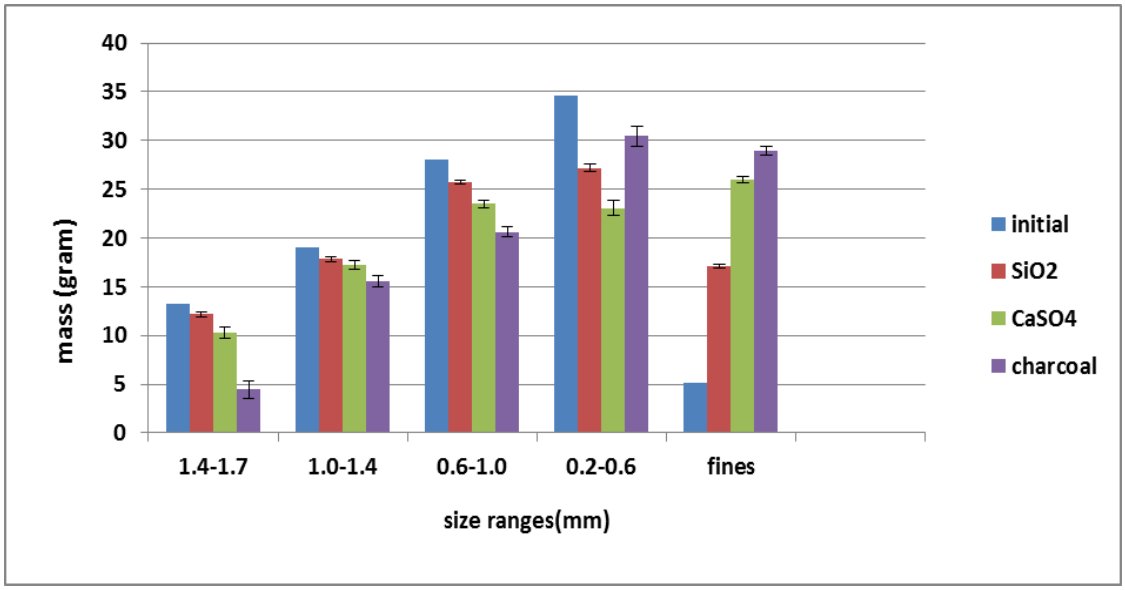

Fig. 14. Remaining mass of three materials (activated charcoal, gypsum and silicon dioxide) after 20 hours.

Silicon dioxide, anhydrous gypsum and activated charcoal are all run to 20 hours at the same excess gas velocity (0.59 m/s and 0.89 m/s) with the same starting particle size distribution. In Figure 14, remaining mass of three materials at excess gas velocity (0.59 m/s) as well as the initial condition is plotted across all size ranges. The situation of excess gas velocity 0.59m/s shows the same trend with excess gas velocity of 0.89 m/s except that 0.89 m/s excess gas velocity will have more attrition in each material and each size ranges; hence the situation of 0.59 m/s is only shown and discussed here. In size range of 1.4-1.7 mm, 1.0-1.4 mm and 0.6-1.0 mm, they show the same trend that charcoal shows more reduction than the other two materials and $CaSO_4$ shows more attrition than SiO_2. In generation of fines, it shows reverse trend. Given that the hardness of three materials are in descending order as silicon dioxide (mohs hardness 7) > anhydrous gypsum (mohs hardness 3.5) > activated charcoal (mohs hardness 1-2) [64], it reveals that attrition decrease with increasing hardness of material at end of run. Unlike other four size ranges, it shows different trend in size range of 0.2-0.6 at both excess gas velocity (0.59 m/s, 0.89 m/s). In Figure 14, mass of charcoal is more than other two materials in the size range of 0.212-0.6 mm. It was reported that soft and coarse particle like activated charcoal will behave in following manner in fluidized bed when superficial gas velocity is at least three times bigger than minimum fluidization velocity. The mother particle will be more likely to undergo particle breakage to form intermediate sized particle before they becomes finely sized

particle [18]. In this case, big charcoal particle is believed to undergo particle breakage to form small sized particle (0.2-0.6 mm) first and subsequently attrited to fine particles. Due to fragmentation of big particles of charcoal, there will be a built-up of 0.2-0.6 mm particles. This surge of 0.2-0.6 mm charcoal particle will at some point offset destruction of them. It could possibly explain the higher mass of 0.2-0.6 mm sized activated charcoal particle at end of run. While the other two material are harder than charcoal, they will be less likely to form intermediate particle through breakage. Therefore they will not have built- up of 0.2-0.6 mm sized particle and shows lower mass at end of run than charcoal.

5.2.2.2. Attrition of 1.4-1.7 mm particle of three materials with time

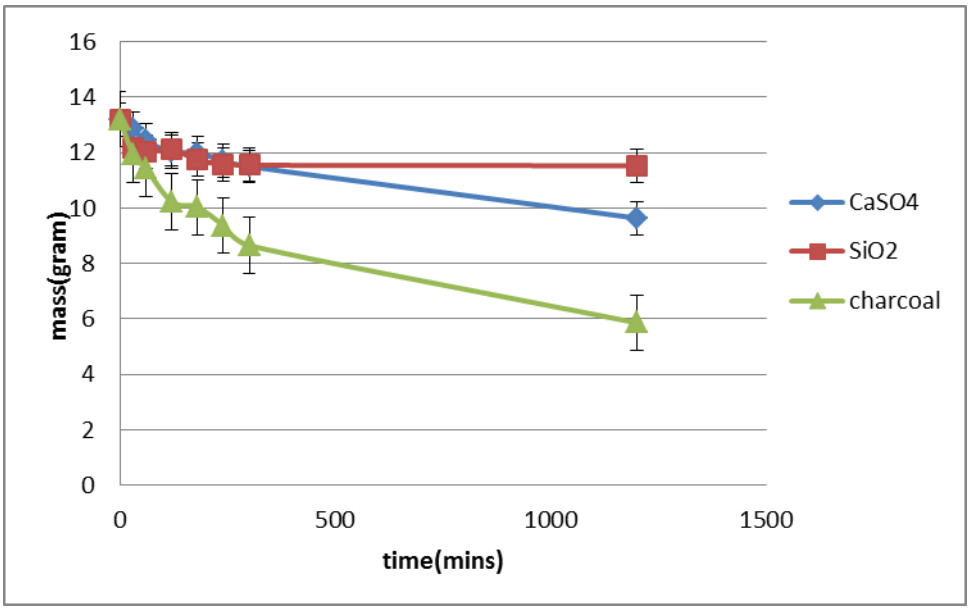

Fig. 15. Attrition of 1.4-1.7 mm particle size of three materials with time (20 h).

In figure 15, mass changes of 1.4-1.7mm sized particle of three materials are plotted against the whole timescale. The slope of lines demonstrates that attrition of each material is rapid at first and gradually decreases which is consistent with the findings in IBA and literature [61]. It is also worth noting that mass of charcoal is much lower than the other two materials during the whole process. It indicates that charcoal is attrited vigorously. Furthermore, the lines representing attrition of anhydrous gypsum and silicon dioxide are found to overlap with each other in the beginning, however, silicon dioxide shows little change afterwards until 20 hours and

anhydrous gypsum shows more change happens at later stage. In figure 16, attrition of 1.4-1.7mm particle size of three materials are shown in the short run (5h).

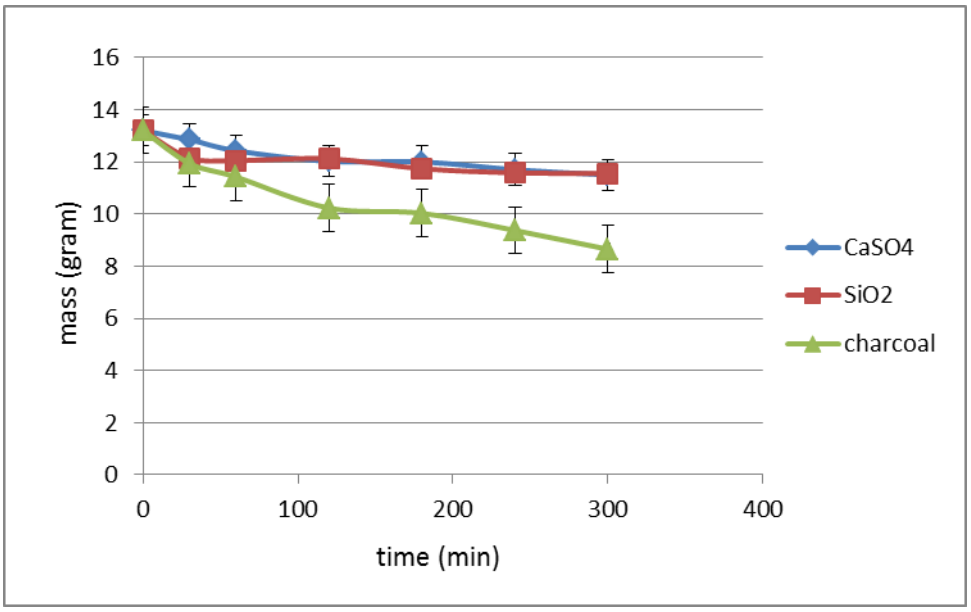

Fig. 16. Attrition of 1.4-1.7 mm particle size of three materials with time (5 h).

In Figure 16, it clearly reveals the attrition of $CaSO_4$ and SiO_2 behave in a similar manner before five hours although they differ much in hardness. CaSO4 is with 3.5 mohs hardness while SiO2 is much harder than that with 7 mohs hardness. It could be explained two reasons as below.

1) It is known that anhydrous gypsum (CaSO4) is widely used as desiccant. It will slowly absorb moisture in the air. On a side experiment, 14.23 gram of $CaSO_4$ is put into beaker in the lab. The mass change of it is recorded in table 3. The results show that it will absorb less than 0.2g moisture in the air every hour in the beginning. Although attrition will reduce mass while absorption of water will increase mass, the actual attrited mass will appear to be slightly underestimated in the figure.

Table 7. Mass change of CaSO4 with time (20 h) in the air.

0h	1h	2h	3h	20h
14.23g	14.42g	14.58g	14.67g	15.09g

2) It was reported that attrition in the beginning is due to loose particles, sharp edge and corner as well as cracks [63]. By definition, hardness is a measurement of resistance to localized plastic deformation. Hence material with higher hardness will be less likely to undergo localized plastic deformation under stress. Attrition occurs by inter-particle movement (collision, sliding). Local loading will give rise to plastic deformation which will further develop into either subsurface lateral or radial crack. Subsurface lateral crack contributes most to attrition while radial crack cannot propagate further into core so it will not contribute. Under stress, subsurface lateral crack will be activated and propagate and finally lead to attrition of material. It is easy to form a crack and propagate on sharp edge and corner in the beginning because of small radius of curvature [65]. For SiO_2 which has mohs hardness 7, it is very hard for SiO_2 to generate a localized plastic deformation at later stage. Therefore it is extremely hard to be further attrited once pre-existing flaws are all propagated and sharp edges are removed. That explains SiO_2 shows little change after five hours. For $CaSO_4$ which has smaller hardness than SiO_2, it is easier for them to undergo plastic deformation under stress than SiO_2 thus stand more chance to form crack. But it is also reported that crack will only propagate when threshold strength is reached [66]. Particles inside fluidized bed are constantly interacting with each other. Some particles are colliding each other; some particles are sliding over each other, some particles are rolling over each other. Each interaction pattern will give rise to different strength and not every interaction can exceed threshold strength to initiate crack. Therefore crack will take longer time to propagate especially for materials with higher hardness. It can be inferred that in this case gas velocity cannot provide sufficient energy for subsurface crack to propagate in $CaSO_4$. So subsurface crack cannot readily propagate to lead to attrition of material in the first. It also explains why $CaSO_4$ shows much increased attrition rate after five hours compared to SiO_2.

5.2.2.3. Percentage of change of 1.4-1.7 mm of three materials

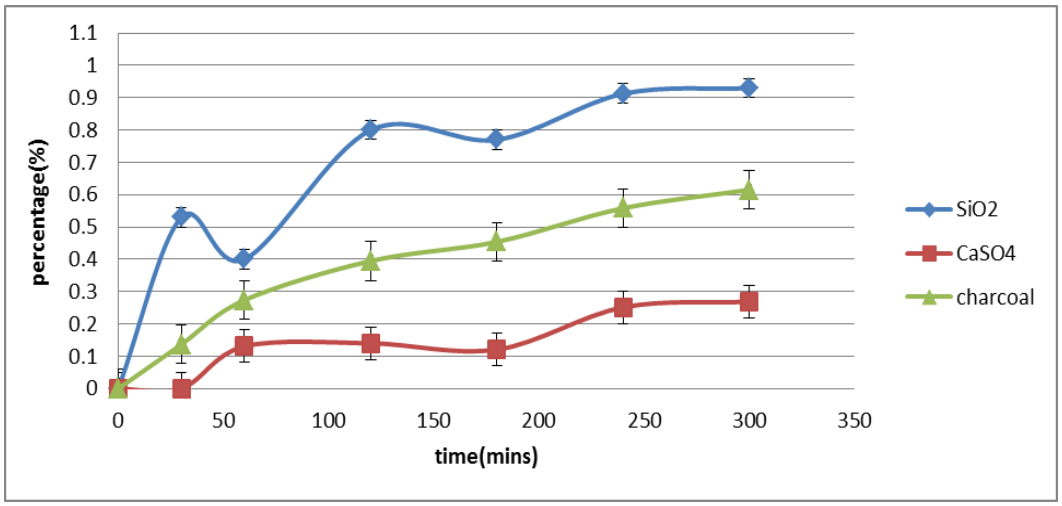

Fig. 17. The percentage of total change of 1.4-1.7 mm of three materials with time (5h).

In Figure 17, the percentages of total change of 1.4-1.7 mm of three materials are plotted against time. The percentage of attrition is defined as the ratio of the amount of change between beginning to preset time (0.5h, 1h, 2h, 3h, 4h, and 5h) to total change from beginning to end of run (20h). It reveals how fast attrition is taking place across whole timescale. The blue line which represents percentage of total change of SiO_2 is far above the other two lines and the green one representing charcoal is distinctively above that of $CaSO_4$. It is worthy nothing that 50% of total change for SiO_2 happens within half an hour and surprisingly 90% of total change happens in four hours, however, only 10% happens for the remaining sixteen hours. It proves again that SiO_2 cannot be further attrited with time from other perspective since it has very high hardness. It reaches equilibrium state much faster than other two materials. It can be inferred that the higher attrition at beginning results from easy breakage of loose particle, sharp edge and corners. On an another note, The sudden drop in percentage of silicon dioxide at one hour is mainly due to fluctuation of mass stemming from sieving machine. The mass of 1.4-1.7mm at one hour was supposed to decrease after half hour. But considering the sieving machine works by vigorously shaking those particles through their different meshes and is subject to working efficiency. It is understandable that it cannot separate particles between two adjacent meshes perfectly. It should be noted the starting mass is 13.2g, the mass at half an hour is 12.67g, and the mass at one hour is 12.78g. 12.78 is a little higher than 12.67, so there is sudden drop in percentage of silicon dioxide.

The percentage of change of $CaSO_4$ increases to around 10% after one hour and remains nearly constant for another two hours and subsequently increases to around 30% at fifth hour. It looks like attrition is paused in the middle and re-starts to increase afterwards. More than 70% of total change happens in the next fifteen hours. It shows consistence with suggestion before that attrition is slowed down at first because crack formation and propagation will take time for anhydrous gypsum. Furthermore, loose particle and sharp edges is believed to be attrition source in the beginning. The green line representing percentage of change of charcoal reveals that around 30% change happens in the first hour and 60% change happens in first five hours and only 40% happens in the following fifteen hours. It changes in a continuous way. Compared to red line which represents gypsum, the red line is steeper and higher. It indicates the attrition of activated charcoal is happening faster than attrition of gypsum in the first place. It could be due to low hardness and high porosity. Porosity is found to make material weak and more prone to attrition as reported in literature. [34] By means of high porosity in gypsum, current gas velocity is sufficient strong to attrite charcoal constantly and smoothly.

5.2.2.4. Generation of fines of three materials with time (20 h)

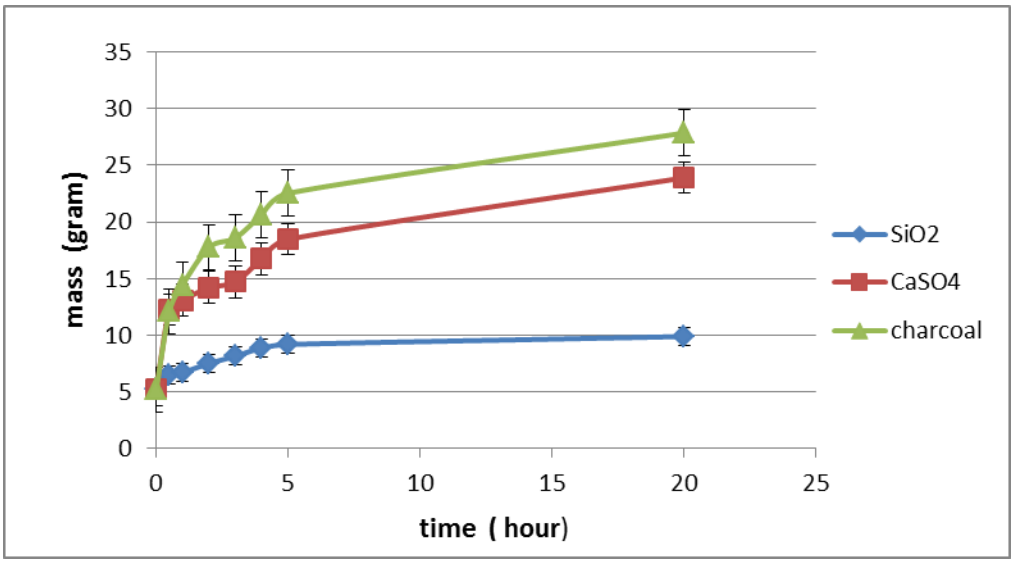

Fig. 18. Generation of fines of three materials with time (20 h).

In figure 18, for three materials, the generation of fine is very rapid at first then gradually slows down. Abrasion is believed to be the dominant mechanism in fluidized

bed so production of fines reveals the extent of abrasion. So looking into generation of fines can provide an insight into the extent of attrition of material. After five hours, generation of fines of SiO_2 remains almost constant until 20 hours. It is consistent with the behavior which is shown in attrition of 1.4-1.7mm particle. It also demonstrates that the other sizes of SiO_2 particles show the same reluctance to attrition after five hours as 1.4-1.7mm. While the other materials keep increasing and charcoal ends up producing more fines than $CaSO_4$ at end of run. At first stage, the generation of $CaSO_4$ behaves closely with that of SiO_2. It is possibly due to easy breakage of pre-existing flaws in each size of them that makes them produce fine in a similar manner. However, the fines of $CaSO_4$ are further generated due to crack propagation at later stage. Surprisingly, at first five hours, the generation of fines of charcoal is only slightly higher than the other two. It seems to contradict the trend shown in attrition of 1.4-1.7mm that charcoal is attrited much more than other two materials. It is possibly due to the fragmentation of big charcoal particle into small sized particle. So instead of abrasion which generates fines, it will break into intermediate sized particle hence reducing generation of fines. It is reported that fragmentation will be likely to happen in distributor area due to formation of jet [67] and activated charcoal is likely to undergo breakage to intermediate sized particles first. [34]

6. Conclusions

Glass beads were introduced to co-fluidize with IBA at 1.3m/s to study the effect of different sizes and different compositions of glass beads on the attrition of IBA. It is found that attrition rate will increase dramatically in the beginning and then gradually level off to a plateau because fragile structure like sharp corner and edges will be destroyed in the first place. It also shows more significant reduction of mass (i.e., attrition of IBA) in size range of 1.4-1.7 mm with addition of glass beads due to increased contact surface area resulting from addition of glass beads. Addition of glass beads is also revealed to generate fines faster thus to show higher attrition rate. In terms of generation of fines, it will be related to two competing factors: contact surface area and energy density (energy acting on unit area). Increased contact surface area will enhance surface area exposed to attrition. Energy density means impacting energy acting on unit area. Impacting energy is believed to share between surface areas. The more contact surface areas are, the less impacting energy is acting on unit area. Small glass beads (0.212-0.6mm) will produce more fines in the first place than medium glass beads (0.6-1.0mm) because small glass beads have more contact surface area and increased contact surface area will become dominant factor in chipping away fragile structure in the first place. Medium glass beads which have more energy density will produce fewer fines in the first but eventually produce more fines. Because after fragile structure and pre-existing flaws are eliminated, it will need more energy for further attrition. However, due to inhomogeneous physical properties of IBA and introduction of foreign particles, experimental results will be prone to big discrepancy. The following study was focused on study attrition of three materials which are physically and chemically homogeneous. There materials are silicon dioxide, anhydrous gypsum and activated charcoal. Furthermore, the effect of gas velocity and hardness on attrition of three materials was investigated. It was found that gas velocity will have noticeable influence on attrition of 1.4-1.7mm particle size and attrition is shown to increase with gas velocity. But it shows little influence on other particle size ranges possibly because the chosen gas velocity interval is small. Secondly, material hardness is found to have remarkable influence on attrition of materials. It is found that attrition will decrease with increased material hardness. In attrition of biggest particle size (1.4-1.7mm), attrition of charcoal which has lowest hardness is much bigger than

other two materials due to high porosity and low hardness. Silicon dioxide shows the similar behavior with anhydrous gypsum in the first five hours due to easy breakage of pre-existing flaws or fragile structure. While silicon dioxide shows little change after it and anhydrous gypsum is revealed to have more change in the latter stage. It is possibly because crack in anhydrous gypsum cannot readily propagate in the first place and crack formation and propagation takes time, it shows more change at latter stage. Silicon dioxide which has highest hardness among three materials cannot generate more crack thus cannot be further attrited. In terms of generation of fines, materials with higher hardness end up generating fewer fines while silicon dioxide stops generating fines after first five hour and other two are still increasing. Activated charcoal shows slightly more fine than other two materials, it is possibly due to fragmentation of particle to intermediate size thus reduce generating of fines.

7. Reference

1. Khoo, H.H., L.L.Z. Tan, and R.B.H. Tan, *Projecting the environmental profile of Singapore's landfill activities: Comparisons of present and future scenarios based on LCA.* Waste Management, 2012. **32**(5): p. 890-900.
2. Li, M., et al., *Characterization of solid residues from municipal solid waste incinerator.* Fuel, 2004. **83**(10): p. 1397-1405.
3. Hjelmar, O., *Disposal strategies for municipal solid waste incineration residues.* Journal of Hazardous Materials, 1996. **47**(1–3): p. 345-368.
4. Kirby, C.S. and J.D. Rimstidt, *Mineralogy and surface properties of municipal solid waste ash.* Environmental Science & Technology, 1993. **27**(4): p. 652-660.
5. Belevi, H. and H. Moench, *Factors Determining the Element Behavior in Municipal Solid Waste Incinerators. 1. Field Studies.* Environmental Science & Technology, 2000. **34**(12): p. 2501-2506.
6. Jung, C.H., et al., *Metal distribution in incineration residues of municipal solid waste (MSW) in Japan.* Waste Management, 2004. **24**(4): p. 381-391.
7. Yao, J., et al., *Content, mobility and transfer behavior of heavy metals in MSWI bottom ash in Zhejiang province, China.* Fuel, 2010. **89**(3): p. 616-622.
8. Zhang, H., P.-J. He, and L.-M. Shao, *Fate of heavy metals during municipal solid waste incineration in Shanghai.* Journal of Hazardous Materials, 2008. **156**(1–3): p. 365-373.
9. Eighmy, T.T., et al., *Particle petrogenesis and speciation of elements in MSW incineration bottom ashes*, in *Studies in Environmental Science*, J.J.J.M. Goumans, H.A. van der Sloot, and T.G. Aalbers, Editors. 1994, Elsevier. p. 111-136.
10. Jung, C.H., et al., *Metal distribution in incineration residues of municipal solid waste (MSW) in Japan.* Waste Manag, 2004. **24**(4): p. 381-91.
11. Yao, Q.J., et al., *Mobility of heavy metals and rare earth elements in incineration bottom ash through particle size reduction.* Chemical Engineering Science, 2014. **118**: p. 214-220.
12. Werther, J. and J. Reppenhagen, *Attrition*, in *Handbook of Fluidization and Fluid-Particle Systems*, W.C. Yang, Editor. 2003, Marcel Dekker, Inc: New York, USA.
13. Pis, J.J., et al., *Attrition of coal ash particles in a fluidized-bed.* Powder Technology, 1991. **66**(1): p. 41-46.
14. Ray, Y.C., T.S. Jiang, and C.Y. Wen, *Particle attrition phenomena in a fluidized-bed.* Powder Technology, 1987. **49**(3): p. 193-206.
15. Patience, G.S. and P.L. Mills, *Modelling of propylene oxidation in a circulating fluidized-bed reactor*, in *Studies in Surface Science and Catalysis*, V.C. Corberán and S.V. Bellón, Editors. 1994, Elsevier. p. 1-18.
16. Merrick, D. and J. Highley, *Particle size reduction and elutriation in a fluidized bed process.* AIChE, 1974: p. 367-378.
17. Clift, R., *Powder technology and particle science.* Powder Technology, 1996. **88**(3): p. 335-339.
18. Blinichev, V.N., V.V. Streltso, and E.S. Lebedeva, *An investigation of size reduction of granular materials during their processing in fluidized beds.* International Chemical Engineering, 1968. **8**(4): p. 615-618.
19. Pell, M., *Gas fluidization*, in *Handbook of Powder Technology*. 1990, Elsevier: Amsterdam. p. 97-106.
20. Reppenhagen, J. and J. Werther, *Catalyst attrition in cyclones.* Powder Technology, 2000. **113**(1-2): p. 55-69.
21. Zenz, F.A., *Find attrition in fluid beds.* Hydrocarbon Processing, 1971. **50**(2): p. 103-&.
22. Werther, J. and J. Reppenhagen, *Catalyst attrition in fluidized-bed systems.* AIChE Journal, 1999. **45**(9): p. 2001-2010.

23. Kutyavina, T.A. and A.P. Baskakov, *Grinding of fine granular material with fluidization.* Chem Techn Fuels Oils, 1972. **8**: p. 210-213.
24. Contractor, R.M., et al. *Attrition resistant catalysts for fluidized bed-systems*. in *Fluidization VI*. 1989. New York: Engineering Foundation.
25. Arastoopour, H. and C.Y. Chen, *Attrition of char agglomerates.* Powder Technology, 1983. **36**(1): p. 99-106.
26. Seville, J.P.K., M.A. Mullier, and M.J. Adams. *Attrition of agglomerates in fluidized beds*. in *Fluidization VII*. 1992. New York: Engineering Foundation.
27. Ghadiri, M., J.A.S. Cleaver, and K.R. Yuregir. *Attrition of sodium chloride crystals in a fluidized bed*. in *Fluidization VII*. 1992. New York: Engineering Foundation
28. Werther, J. and W. Xi, *Jet attrition of catalyst particles in gas-fluidized beds.* Powder Technology, 1993. **76**(1): p. 39-46.
29. Arena, U., M. Damore, and L. Massimilla, *Carbon Attrition during the Fluidized Combustion of a Coal.* Aiche Journal, 1983. **29**(1): p. 40-49.
30. Kono, H., *Attrition rates of relatively coarse solid particles in various types of fluidized beds*. 1981, AIChE. p. 96-106.
31. Zenz, F.A., *Help from project E-A-R-L.* Hydrocarbon Processing, 1974. **53**(4): p. 119-124.
32. Zenz, F.A. and G.H. Kelleher, *Studies of attrition rates in fluid-particle systems via free fall, grid jets, and cyclone impact.* Journal of Powder Bulk Technology 1980. **4**(13-20).
33. Boerefijn, R., S.H. Zhang, and M. Ghadiri, *Analysis of ISO fluidised bed jet test for attrition of fluid cracking catalyst particles.* Fluidization Ix, 1998: p. 325-332.
34. Bemrose, C.R. and J. Bridgwater, *A review of attrition and attrition test methods.* Powder Technology, 1987. **49**(2): p. 97-126.
35. Wu, S.Y., J. Baeyens, and C.Y. Chu, *Effect of the grid-velocity on attrition in gas fluidized beds.* Canadian Journal of Chemical Engineering, 1999. **77**(4): p. 738-744.
36. Forsythe, W.L. and W.R. Hertwig, *Attrition Characteristics of Fluid Cracking Catalysts - Laboratory Studies.* Industrial and Engineering Chemistry, 1949. **41**(6): p. 1200-1206.
37. Tomeczek, J. and P. Mocek, *Attrition of coal ash particles in a fluidized-bed reactor.* AIChE Journal, 2007. **53**(5): p. 1159-1163.
38. Dessalces, G., F. Kolenda, and J.P. Reymond, *Attrition evaluation for catalysts used in fluidized or circulating fluidized bed reactors*, in *Preprints of the First International Particle Technology Forum, Part II*. 1994: Denver, CO. p. 190-196.
39. Gwyn, J.E., *On particle size distribution function and attrition of cracking catalysts.* AIChE Journal, 1969. **15**(1): p. 35-38.
40. Anthony, E.J. and D.L. Granatstein, *Sulfation phenomena in fluidized bed combustion systems.* Progress in Energy and Combustion Science, 2001. **27**(2): p. 215-236.
41. Rhodes, M., *Particle size reduction*, in *Introduction to Particle Technology*, M. Rhodes, Editor. 2008, John Wiley & Sons, Ltd.: Hoboken. p. 311-333.
42. Williams, J.A., *Analytical models of scratch hardness.* Tribology International, 1996. **29**(8): p. 675-694.
43. Yang, W.C., *Flow through fixed beds*, in *Handbook of Fluidization and Fluid-Particle Systems*, W.C. Yang, Editor. 2003, Marcel Dekker, Inc: New York, USA.
44. Wredenberg, F. and P.L. Larsson, *Scratch testing of metals and polymers: Experiments and numerics.* Wear, 2009. **266**(1-2): p. 76-83.
45. Rockwell, H.M. and S.P. Rockwell, *Hardness-tester*. 1919, Google Patents.
46. Pavlina, E.J. and C.J. Van Tyne, *Correlation of yield strength and tensile strength with hardness for steels.* Journal of Materials Engineering and Performance, 2008. **17**(6): p. 888-893.
47. Tietze, M. and M. Kompatscher, *Predicative hardness testing for production control and materials design*. 2002, IMEKO.

48. Chen, C.-K., et al., *Size distribution of metals in bottom ash of municipal solid waste incinerators.* J. Environ. Eng. Manag, 2008(18): p. 105-113.
49. Menendez-Diaz, J.A., I. Martin-Gullon, and T.J. Bandosz, *Activated Carbon Surfaces in Environmental Remediation*. 2006, Elsevier: The Netherlands. p. 1-47.
50. Henning, K.-D. and H. von Kienle, *Carbon, 5. Activated Carbon*, in *Ullmann's Encyclopedia of Industrial Chemistry*. 2010.
51. Cecen, F., *Activated Carbon*, in *Kirk-Othmer Encyclopedia of Chemical Technology*. 2014, John WIley & Sons, Inc. p. 1-34.
52. Rodriguez, F.-R., *Production and Applications of Activated Carbons*, in *Handbook of Porous Solid*, F. Schuth, K.S.W. Sing, and J. Weitkamp, Editors. 2002, John Wiley & Sons: Weinheim, Germany. p. 1766-1827.
53. Suzuki, M., *Adsorption Engineering*. 1990, Tokyo, Japan: Elsevier.
54. Sontheimer, H., J. Crittenden, and R.S. Summers, *Activated Carbon for Water Treatment*. 1988, Germany: Karlsruhe University.
55. Marsh, H. and F. Rodriguez-Reinoso, *Activated Carbon*. Elsevier Science & Technology Books. 2006: Elsevier.
56. McEnaney, B., *Properties of Activated Carbons*, in *Handbook of Porous Solid*, F. Schuth, K.S.W. Sing, and J. Weitkamp, Editors. 2002, John Wiley & Sons: Weinheim, Germany. p. 1828-1863.
57. Fernández, L.D., E. Lara, and E.A.D. Mitchell, *Checklist, diversity and distribution of testate amoebae in Chile.* European Journal of Protistology, 2015. **51**(5): p. 409-424.
58. El-Kareh, B., *Fundamentals of Semiconductor Processing Technologies*. 1995: Kluwer Academic Publishers.
59. Gangolli, S., *The Dictionary of Substances and Their Effects: C*. 1999: Royal Society of Chemistry.
60. Lide, D.R., *CRC Handbook of Chemistry and Physics*. 71 ed. 1991, Boca Raton: CRC Press, Inc.
61. Cook, J.L., et al., *Attrition and changes in particle size distribution of lime sorbents in a circulating fluidized bed absorber.* Powder Technology, 1996. **89**(1): p. 1-8.
62. Arena, U., et al., *Carbon attrition in the fluidized combustion of a metallurgical coke.* Combustion and Flame, 1984. **57**(1): p. 123-125.
63. Chen, Z., J.R. Grace, and C. Jim Lim, *Limestone particle attrition and size distribution in a small circulating fluidized bed.* Fuel, 2008. **87**(7): p. 1360-1371.
64. Ludema, K.C., *Strength and deformation properties of solids*, in *Friction, Wear, Lubrication: A Textbook in Tribology*. 1996, CRC Press. p. 27.
65. Ghadiri, M. and Z. Zhang, *Impact attrition of particulate solids. Part 1: A theoretical model of chipping.* Chemical Engineering Science, 2002. **57**(17): p. 3659-3669.
66. Lawn, B.R. and T.R. Wilshaw, *Fracture of Brittle Solids*. 1975: Cambridge University Press.
67. Vaux, W.G. and A.W. Fellers, *Measurement of attrition tendency in fluidization*. 1981, AIChE. p. 107-115.